THESIS

A STUDY OF SIMULATED NEUTRONS IN THE NOνA NEAR DETECTOR

Submitted by

Jessica Jarosz

Department of Physics

In partial fulfillment of the requirements

For the Degree of Master of Science

Colorado State University

Fort Collins, Colorado

Fall 2020

Master's Committee:

Advisor: Norm Buchanan

Robert Wilson
Kirsten Eilertson

ABSTRACT

A STUDY OF SIMULATED NEUTRONS IN THE NOνA NEAR DETECTOR

This thesis explores how neutron interactions can be studied in the NOνA near detector, and the potential use of a deuterium-tritium neutron source. Understanding neutron kinematics within the near detector could aid in constraining antineutrino properties in charged-current quasi-elastic interactions. Refining our knowledge of such an interaction decreases systematic uncertainties, which is crucial for precise neutrino oscillation measurements. Monte-Carlo simulations of mono-energetic neutrons were performed to examine energy deposition, scattering, and neutron energy loss mechanisms.

ACKNOWLEDGEMENTS

This work would not have been possible without the unwavering support I received from many people throughout my graduate career. I would first like to thank my advisor Norm Buchanan for being a committed mentor—not only while writing this thesis, but also as I was going through coursework.

I would also like to thank all of my fellow CSU NOνA contributors, who have consistently been wonderful resources to have whenever I needed software help. These individuals #include: Anne Christensen, Connor Johnson, Derek Doyle, Paul Rojas, and Steven Calvez. NOνA contributors outside of CSU were also of tremendous help in getting my questions answered, especially Teresa Lackey and Miranda Elkins. I would still be banging my head against the keyboard if it weren't for these individuals.

A final, and the biggest of thank yous, goes to my family. They were always there to pick me up when I was down, and never questioned my ambitions or dreams. I would not be the person I am today without them.

TABLE OF CONTENTS

LIST OF TABLES

LIST OF FIGURES

Chapter 1

Introduction

In 1932, physicist Sir James Chadwick made "one of the most significant discoveries of the twentieth century" [1]—he discovered the neutron. Neutrons possess a very important characteristic in that they are electrically neutral. This allows for the neutron to pass unhindered into a nucleus, which presents interesting consequences in various fields of science, from particle physics to medicine. Neutrons can be used to induce fission reactions, which was the catalyst behind the detonation of the first atomic bomb in 1945. They can also be used to penetrate into cancerous cells and rid humans of tumors. In the context of particle physics, they can hold the key to understanding the strong force that holds nuclei together.

For this study, neutrons are analyzed for their role in antineutrino interactions. Antineutrinos and neutrinos are fundamental particles that exist within our Universe. They are both electrically neutral and mainly interact via the weak interaction. These properties make neutrinos experimentally invisible and difficult to measure; thus, in order to study them, neutrinos must be analyzed indirectly through their interactions with other particles. One such experiment that studies neutrino properties is the NOνA experiment, based out at the Fermi National Accelerator Laboratory in Batavia, Illinois. The experiment consists of two detectors: the near detector located at the Fermi Lab campus; and the far detector located 810 km away in Ash River, Minnesota. This experiment is designed to study neutrino oscillations. Aside from this, NOνA also seeks to investigate neutrino interactions with matter by passing neutrino or antineutrino beams through the detectors.

In one particular interaction, an antineutrino interacts with a proton, leaving a neutron and charged lepton in the final state. If the proton, neutron, and charged lepton are all well understood, much can be deduced about the antineutrino using conservation principles. Unfortunately, neutrons share a similar problem to neutrinos in that they are invisible in detectors; therefore, in order to resolve any information about the antineutrino in the context of this interaction, the neutron would also need to be studied.

The aim of this study is to analyze a neutron's behavior in the NOνA near detector, focusing on energy deposition, scattering mechanisms, and neutron energy loss. This was performed using Monte Carlo simulations of mono-energetic neutrons incident on the NOνA near detector. Additionally, a cost- and size-conscious deuterium-tritium neutron source was considered for possible implementation of this study.

Chapter 2 gives a background of the neutron and neutrino, as well as their common interaction mechanisms. Also discussed is the motivation behind the study, and the possible deuterium-tritium neutron source considered for experimentation. Details of the NOνA experiment are outlined in Chapter 3. The simulation process used by the NOνA software is explained in Chapter 4. Chapter 5 presents the simulation used in the study as well as the results. The feasibility of using the deuterium-tritium source is also discussed. Finally, a conclusion of this study is done in Chapter 6.

Chapter 2

Motivation

At the most fundamental level, particle physicists study the constituents of matter and radiation, and the interactions between them. These constituents and interactions are summarized using a concise, yet elegant, model known as the Standard Model (SM). Although the SM has had many tremendous successes, it has yet to explain certain observations in physics, for example gravity, dark matter, and the neutrino mass. One particle that may hold the key to understanding these observations, is the neutrino. Neutrinos are neutral leptons that come in three different types, or flavors: electron neutrinos (ν_e), muon neutrinos (ν_μ), and tau neutrinos (ν_τ). They also interact weakly with matter and are now known to have very low mass [23], which makes them difficult to detect; thus, physicists opt to study neutrino interactions with matter. Neutrino interactions can be summarized into two kinds: charged-current (CC) and neutral-current (NC). Given the goal of the NOνA experiment, which is to measure the rate of ν_μ neutrinos oscillating to ν_e neutrinos, CC interactions are of particular importance as they are the desired signals. For one CC interaction involving the antineutrino, the resulting products include a neutron and a positively charged lepton. Unfortunately, this final state neutron can be burdensome to analyze due to its neutral nature. It is thus the goal of this study to analyze the neutron's behavior in the NOνA near detector. From this, it may be possible to infer properties about the antineutrino.

This chapter develops a particle physics background including the Standard Model and the relevant particles to this study. Furthermore, the motivation behind the experiment will be discussed.

2.1 The Standard Model

After more than a century's worth of theory and experimentation, physicists have put together a remarkably sophisticated picture of the fundamental particles that make up matter called the Standard Model (SM) (Figure 2.1). This current model classifies three types of elementary particles: leptons, quarks, and mediators. Leptons consist of six particles and their respective antiparticles:

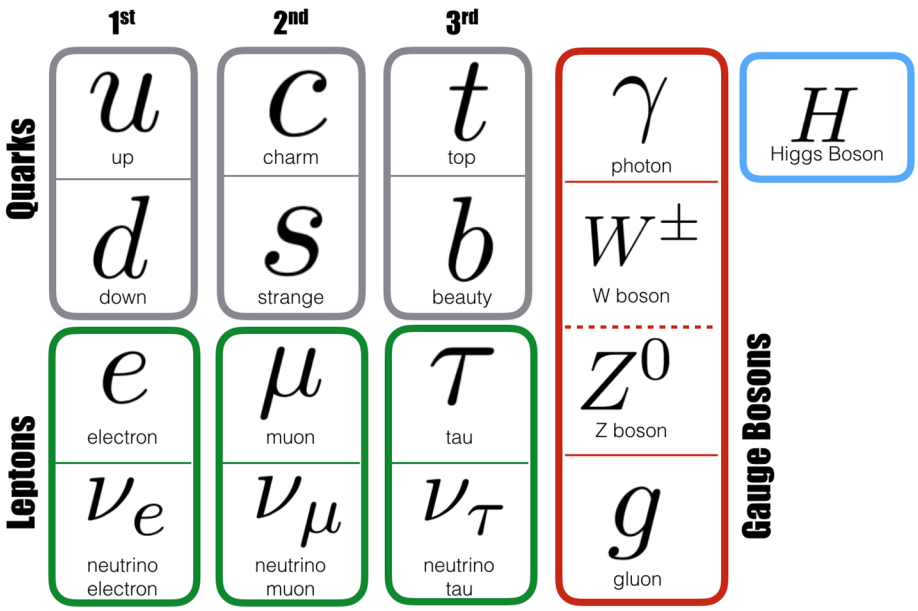

Figure 2.1: Current Standard Model of Particle Physics. Image taken from [7].

the electron, muon, tau, electron neutrino (ν_e), muon neutrino (ν_μ), and tau neutrino (ν_τ). Similarly, there are six flavors of quarks, which are the building blocks of baryons and mesons.

Every interaction is mediated by a force-carrying particle, known as a gauge boson. The SM describes four gauge bosons: the photon, which is responsible for the electromagnetic force, the W and Z bosons for the weak force, and the gluon for the strong force. Finally, the SM includes the recently discovered Higgs Boson [8], which is a particle that gives mass to fundamental particles that interact with it.

2.2 Neutrinos

Of all the SM particles, perhaps the most elusive is the neutrino. Neutrinos primarily interact via the weak interaction—they also interact through the gravitation force, but the relative strength of this force is several orders of magnitude weaker than the weak force [2]. Neutrinos were first theorized before they were experimentally discovered. In the early 1900s, a problem had arisen in the study of nuclear beta decay [24]. In such a decay, it was believed a nucleus decayed into a slightly lighter daughter nucleus, with the emission of an electron. This is an example of a two-

body decay, where one characteristic is that the energies of the resulting particles are kinematically determined and thus should be discrete; however, experimental results showed a continuous distribution for the resulting electron energy. This result was so disturbing, Niels Bohr was ready to abandon the law of conservation of energy [2].

Thankfully, physicist Wolfgang Pauli proposed an alternate theory to reconcile this energy crisis. Instead of this energy being missing, it is possible another particle could be carrying this energy away. The particle would have to be electrically neutral to conserve charge, and would also explain why this particle was not being detected. Shortly after, another scientist, Enrico Fermi, developed a theoretical framework for beta decay that involved Pauli's particle, and thus the neutrino was born [25].

In addition to beta decay, neutrinos can come from a variety of sources including: supernovae, the Big Bang, the sun, reactors, accelerators, and other extragalactic sources. Neutrinos are the second most abundant particle in the Universe, yet they have unknown properties still to be discovered, such as potential CP violation in the neutrino sector and neutrino oscillations. A propagating neutrino does not stick to its flavor state, but rather oscillates between the three and has a certain probability of doing so. Many neutrino experiments are dedicated to pinpointing these exact probabilities of oscillating between the different flavors.

2.3 Charged-Current Interactions

The physics goals that many neutrino experiments aim to achieve require very low systematic uncertainty. This is especially crucial for neutrino oscillation experiments, which typically involve a low data volume of neutrino events in two different detectors. Experiments must be sensitive to small discrepancies in the number of events between the detectors to accurately represent oscillation probabilities. One major source of error in oscillation experiments comes from an improper accounting of all interaction channels neutrinos can take when traversing through matter; thus, much research is going into understanding these interactions and assigning their respective probabilities of occurring.

Neutrino interactions can be classified into one of two categories: CC or NC interactions. CC interactions involved the exchange of a W boson between the incident particles, whereas an NC interaction exchanges a Z boson. Neutrino interactions are also very much energy dependent—a plot of these interaction fractions, or cross sections, as a function of energy can be seen in Figure 2.2. Roughly, a cross section represents the rate of a specific interaction taking place.

The NOνA experiment works to understand all three of the interactions in 2.2: quasielastic scattering, resonance production, and deep-inelastic scattering. Of particular importance in this study, is the charged-current quasi-elastic scattering (CCQE). This type of scattering is described by a neutrino or antineutrino scattering off of a nucleon within a nucleus resulting in a different nucleon in the final state. Additionally, this process is considered quasi-elastic because it possesses both inelastic and elastic qualities. Elastically, the neutrino scatters off a bound nucleon, ejecting another nucleon. An inelastic characteristic is that the initial neutrino is not "conserved", but rather transforms into a charged lepton. There are two ways a CCQE process can occur, one with a neutrino and one with an antineutrino

$$\nu_l + n \rightarrow p + l^- \tag{2.1}$$

$$\bar{\nu_l} + p \rightarrow n + l^+ \tag{2.2}$$

where l could be any of the three types of leptons. Feynman diagrams for both interactions can be seen in Figure 2.3.

2.4 Neutron Cross Sections

Neutrons are of great interest to both nuclear and particle physicists. Due to the neutral nature of the particle, neutrons are unaffected by the Coulomb barrier and can thus traverse through matter much more easily than other nuclear particles. Physicists use this feature of the neutron to study nuclear forces as well as the neutron's role in the nucleus.

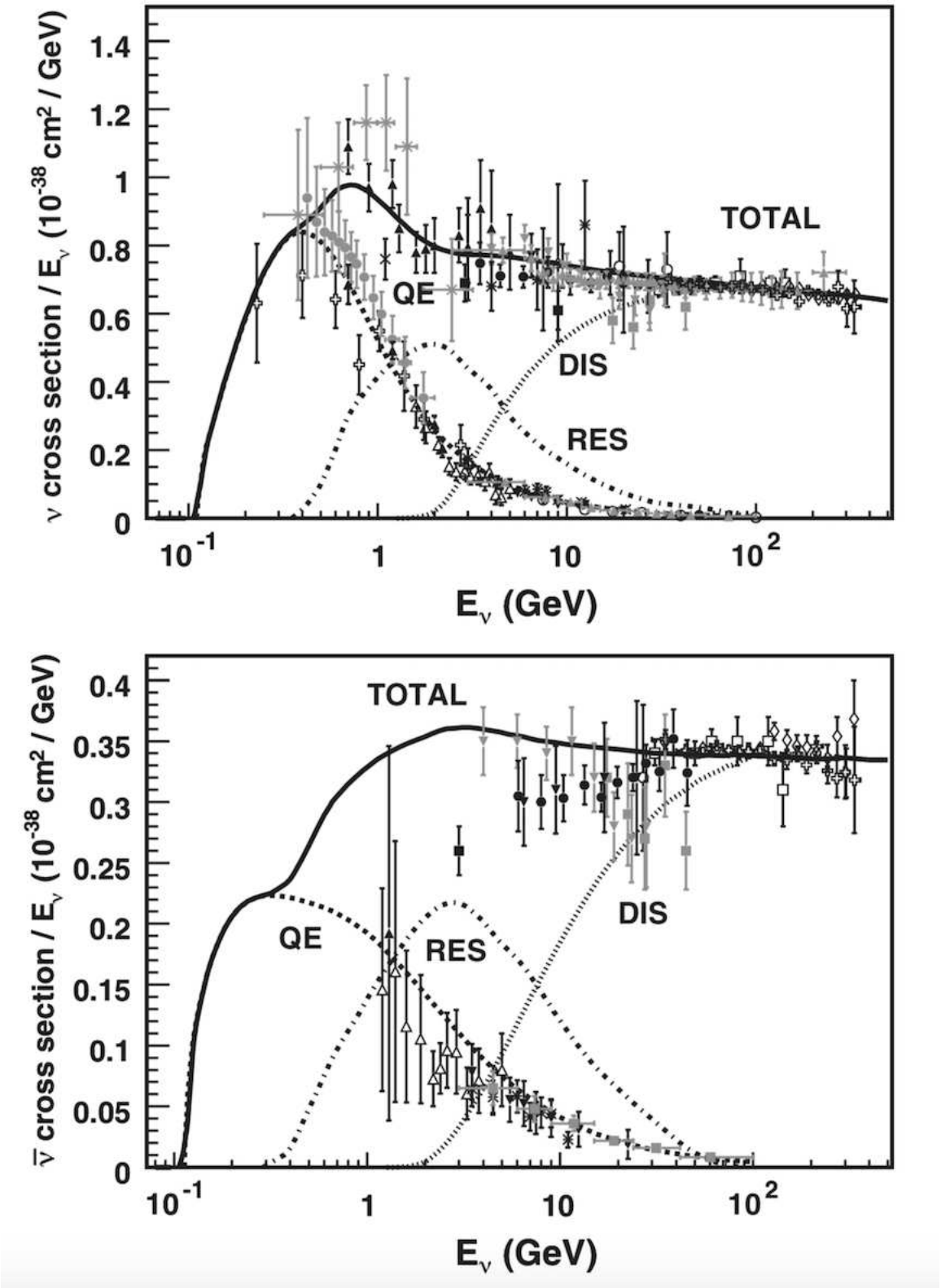

Figure 2.2: Neutrino (top) and anti-neutrino (bottom) cross section per neutrino energy as a function of neutrino energy. Also separated by processes. Contributions include: quasielastic scattering (dashed), resonance production (dot-dashed), and deep-inelastic scattering (dotted). Image taken from [26].

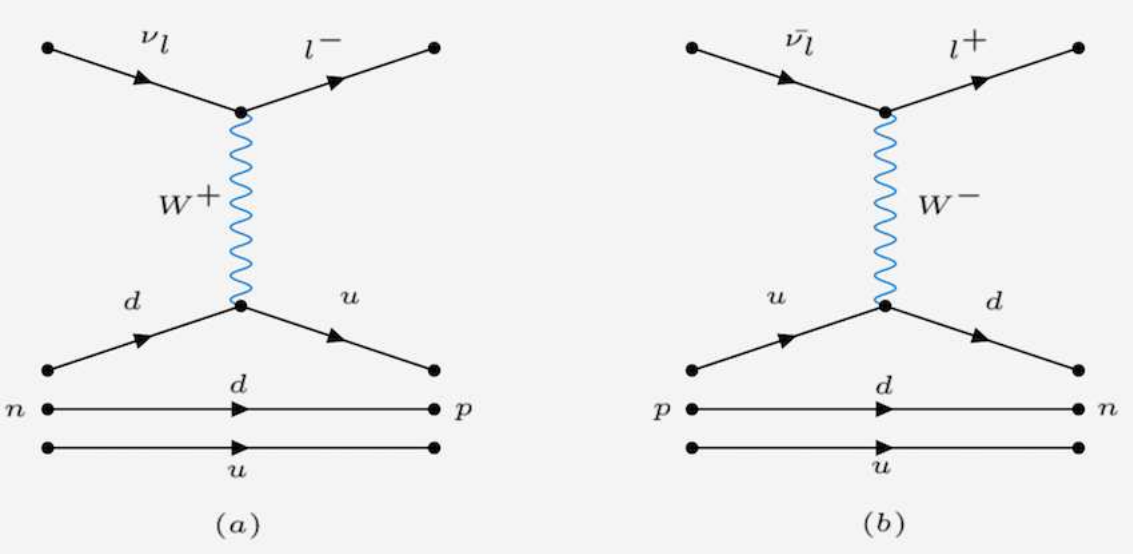

Figure 2.3: Feynman diagrams for CCQE interactions. (a) involves an interaction between a neutrino and neutron while (b) involves a proton and antineutrino.

When studying neutrons, one area of emphasis is in cross section measurements, or the rate of an interaction taking place. The neutron can interact with matter via the following mechanisms:

- Elastic scattering, denoted by (n,elastic)
- Inelastic scattering, denoted by (n,inelastic)
- Neutron capture, denoted by (n,gamma)
- Nuclear fission, denoted by (n, fission)

Each process has a certain rate of occurring which is highly dependent on both the incoming energy of the neutron and the material the neutron is traversing through.

Elastic scattering is a process where the particles going into an interaction are the same particles coming out of the interaction. During the collision, the amount of kinetic energy transferred to the nucleus from the neutron depends on the element. For low atomic number (low Z) materials, the recoil nucleus receives a significant fraction of the incoming neutron's kinetic energy as described by conservation of momentum principles. The resulting scattered neutron is then left with notably less kinetic energy. For high Z materials, the fraction of kinetic energy transferred to the recoil

nucleus is much less, leaving the scattered neutron's kinetic energy marginally affected. Due to this property, low Z materials are commonly used as shielding for fast neutrons (>200 keV).

Another mechanism a neutron can lose energy is inelastic scattering. In this process, a neutron partially transfers its kinetic energy to a nucleus, and some kinetic energy is lost in the excitation of the nucleus. Eventually, this excited nucleus returns to the ground state and emits gamma radiation in the process. Inelastic scattering is a common mechanism for fast neutrons (>200 keV) colliding with high Z materials. The gamma radiation emitted from the de-excitation of the nucleus can range from over one hundred keV to a few MeV.

Neutron capture is another process where a neutron can lose energy. Due to the neutral charge of a neutron, it can penetrate to close proximity of a nucleus, making it a great candidate for capture. Neutron capture is also referred to as a non-elastic collision, as there is no scattered neutron in the final state. Post-capture, nuclear reactions can follow, which can result in the emission of gamma radiation (n,gamma) or other nuclear particles such as protons (n,p), deuterons (n,d), alpha particles (n,alpha), or other neutrons. The type of resulting nuclear reaction is highly dependent on the incident neutron energy as well at the Z of the material. As neutron capture requires the neutron to be in close proximity to the nucleus, this mechanism is more prevalent with slow or thermal neutrons (0.003 eV to 0.4 eV).

A final mechanism in which neutrons can lose energy is from nuclear fission, where a neutron interacts with fissile or fissionable nuclei and then becomes unstable. Following the instability, the nucleus fragments into two nuclei as well as a neutron with relatively high kinetic energy (around 200 MeV). Fission is a process typically reserved for atomic numbers greater than iron—as such, this process is not greatly considered in this study.

Examples of these cross sections can be seen in Figure 2.4 for hydrogen and Figures 2.5 and 2.6 for carbon. Both hydrogen and carbon were considered as the NOνA detectors are themselves hydrocarbon targets. These figures were borrowed from the Evaluated Nuclear Data File (ENDF) [4], which is a library project run by a collaboration of national laboratories, industries, and universities. The most dominant cross section for hydrogen is elastic scattering. Competing with elastic

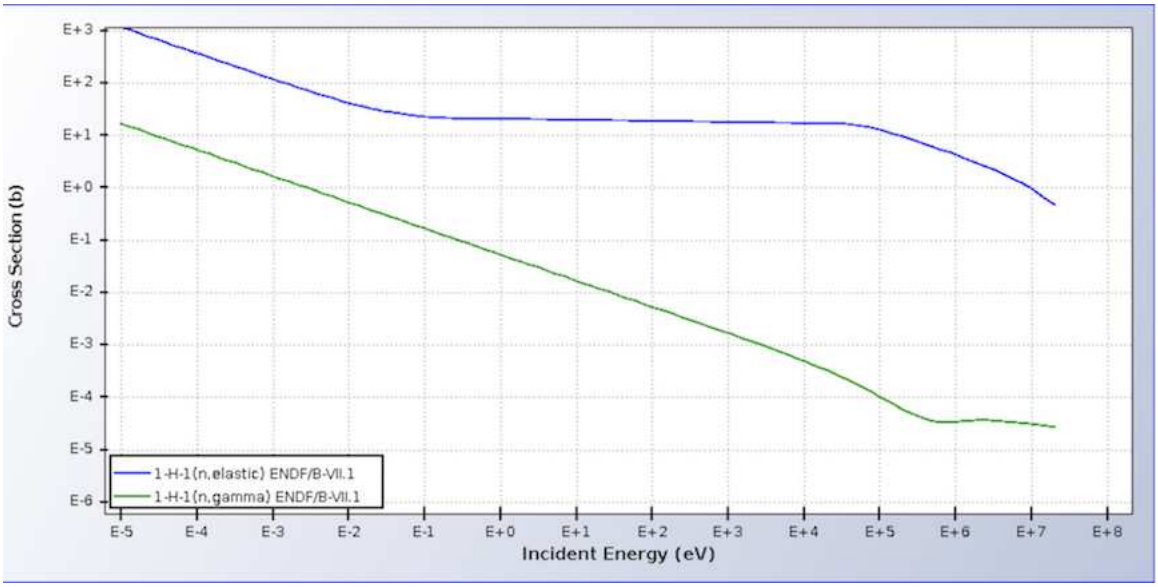

Figure 2.4: Cross section measurements for a neutron with a hydrogen target as a function of incident neutron energy. Elastic is the most dominant mechanism with the probability of such scattering decreasing with incident neutron energy. Plot from ENDF [4].

is (n, gamma) which is the process of neutron capture with the emission of gamma radiation with an energy of 2.23 MeV [10]. As for carbon, it is considered a higher Z material, which is evident by the higher cross section for inelastic scattering at fast incident neutron energies. Additionally, due to the multiple nucleons in carbon, other non-elastic mechanisms are possible and appear to "turn on" at higher incident neutron energies. Typical photon energies for neutron capture or inelastic collision with carbon are 595 keV to about 5 MeV [10].

2.5 Motivation

The neutron's relevance in this study comes from its involvement in CC interactions, more importantly in the case of antineutrino interactions where a neutron is produced in the final state. A neutrino or antineutrino beam incident on a detector is not quite mono-energetic—it is actually comprised of a narrow distribution of energies with long tails. It is possible, however, to constrain this energy using information from the other particles involved. Both the proton and charged lepton energies can be determined as detectors are designed to identify charged particles. This leaves the neutron energy to be deduced. To do this, neutron interactions inside of a detector need to be

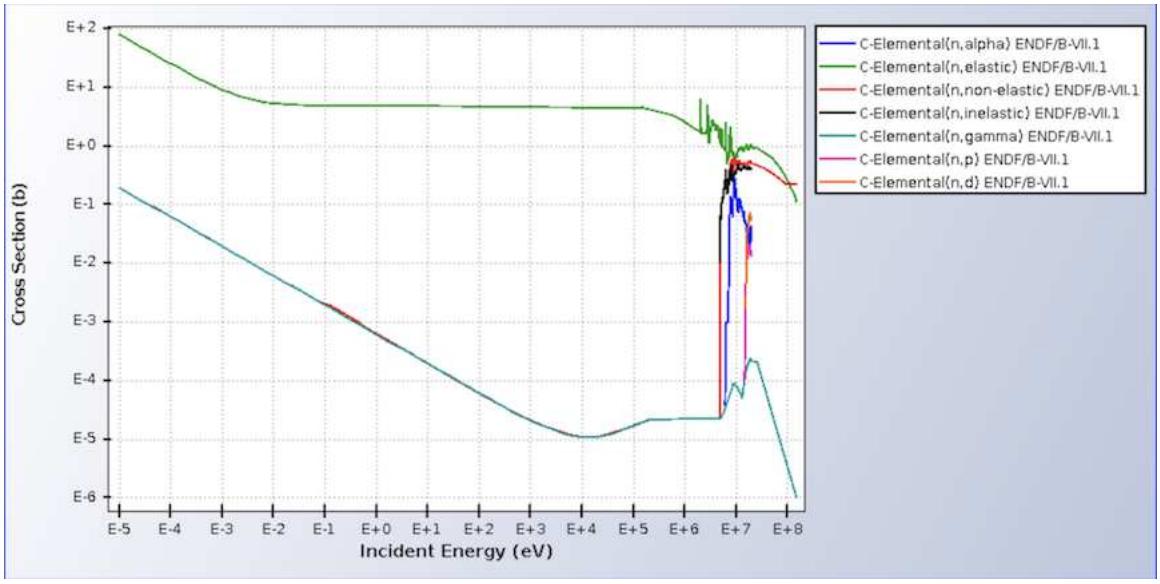

Figure 2.5: Cross section measurements for a neutron with carbon target as a function of incident neutron energy. For lower energies, elastic is the most dominant mechanism. For neutron energies greater than 1 MeV, other processes begin to turn on. Plot from ENDF [4].

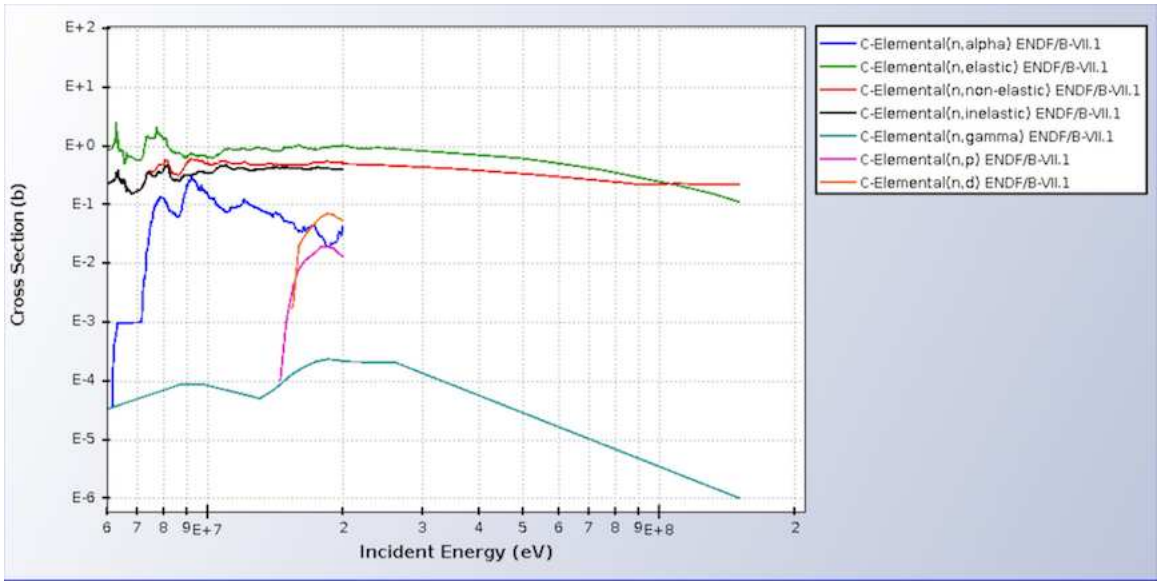

Figure 2.6: Same plot as Figure 2.5, but zoomed in at the higher energies. Non-elastic and inelastic mechanisms become much more prevalent. Plot from ENDF [4].

better understood: how do they deposit energy; how much do they scatter; and what processes are responsible, if any, for the neutron losing energy. The aim of this study is see if such questions can be answered by firing mono-energetic neutrons through a detector. Such studies enable the ability to better determine event energy, especially for antineutrino-nucleus interactions, as well as better identify event types.

2.6 Possible Neutron Source

One source of neutrons considered for possible implementation of this study is a deuterium-tritium (D-T) fusion source, in which either deuterium or tritium is accelerated into the other, resulting in the production of helium and a 14.1 MeV kinetic energy neutron:

$$D + T \rightarrow^{4} He + n \tag{2.3}$$

The benefits to using a D-T neutron source is affordability, compactness of the generator, and very little nuclear waste production compared to nuclear reactors—more importantly, there would not be a nuclear reactor in the vicinity of the detector. Although there are benefits to a D-T neutron source, there are also some downfalls. One main hurdle in using a D-T source is the low operational lifetime of such a device. This is due to the relatively quick depletion of deuterium and tritium within the device. Another issue in using a D-T source, is the neutron beam intensity is relatively low; however, much research and development has gone into improving these drawbacks, which still makes a D-T source worth exploring.

Chapter 3

The NOνA Experiment

As described in the previous chapter, neutrinos rarely interact with other particles, which makes studying them quite challenging. In order to get enough data to analyze how they interact, scientists must create an intense beam of neutrinos and send them through large detectors. An experiment that does exactly this is the NuMI Off-Axis ν_e Appearance (NOνA) experiment. NOνA is a long-baseline neutrino experiment designed to study neutrino oscillations, particularly the rate of ν_μ oscillating to ν_e. Beyond neutrino oscillations, the NOνA collaboration is searching to understand neutrino interactions with matter and even supernova neutrino physics. The NOνA experiment consists of an intense neutrino beam that travels through a near detector (ND) under the Fermilab campus and into a second far detector (FD) approximately 810 km away. Both detectors are arranged 14 mrad off-axis of the beam. Measurements of the electron neutrino rates are then made and compared between the ND and FD to determine the oscillation rate. Additionally, the NuMI beam utilized for the experiment can operate in both neutrino and antineutrino modes to study oscillation properties of both types of particles.

This chapter describes the primary components of the NOνA experiment including the NuMI beam, both near and far detectors, and the data acquisition system.

3.1 NuMI Neutrino Beam

Due to the neutrino's weakly interacting nature, creating a neutrino beam requires an extra layer of ingenuity. The main ingredient needed to create such a beam is a large number of high-energy protons, which originate in Fermilab's Main Injector; hence the name of the neutrino beam utilized by NOνA: Neutrinos at the Main Injector (NuMI) [12].

The Main Injector is a synchrotron accelerator that accelerates protons to 120 GeV for use by various high energy experiments. Batches of these protons are siphoned off and then directed toward a graphite target. These proton-carbon interactions result in the production of charged

mesons, primarily charged pions and kaons. Since charged particles interact with magnetic fields, magnetic horns are used to direct these charged meson in the direction that is desired for the neutrino beam. Eventually, these mesons decay into muons and muon neutrinos by the following most dominant interactions:

$$\pi^+ \rightarrow \mu^+ + \nu_\mu \tag{3.1}$$

$$K^+ \rightarrow \mu^+ + \nu_\mu \tag{3.2}$$

The resulting muons from Equations (3.1) and (3.2) can decay even further via the following dominant channel:

$$\mu^+ \rightarrow e^+ + \nu_e + \bar{\nu_\mu} \tag{3.3}$$

By conservation laws, the resulting neutrinos from (3.1), (3.2), and (3.3) travel along the same direction as the charged mesons did prior to decay, and thus a primarily muon neutrino beam is created. This resulting beam is peaked at 2 GeV.

3.2 Arrangement of NOνA Detectors

Approximately 1 km from the NuMI beam is the NOνA ND, which is located 105 m below ground under the MINOS experiment surface building at the Fermilab campus. Situated 810 km away is the FD near Ash River, MN and is about 200 times more massive than the ND—the ND being 225 ton while the FD is 14 kton. The long distance between the detectors, or long-baseline, allows for an increased probability of the neutrinos oscillating to different flavor states. The energy resolution of the NOνA detectors is around 6-8 MeV.

A unique feature of these detectors is that they are both arranged 14 mrad off axis with respect to the beam center. The purpose of this is to take advantage of the kinematics that govern the pion and kaon decays described previously. When pions and kaons decay, they do so isotropically in the center-of-mass frame which results in a relatively broad neutrino beam energy spectrum. From reference [12], the kinematics of such decays for small angles are found to be:

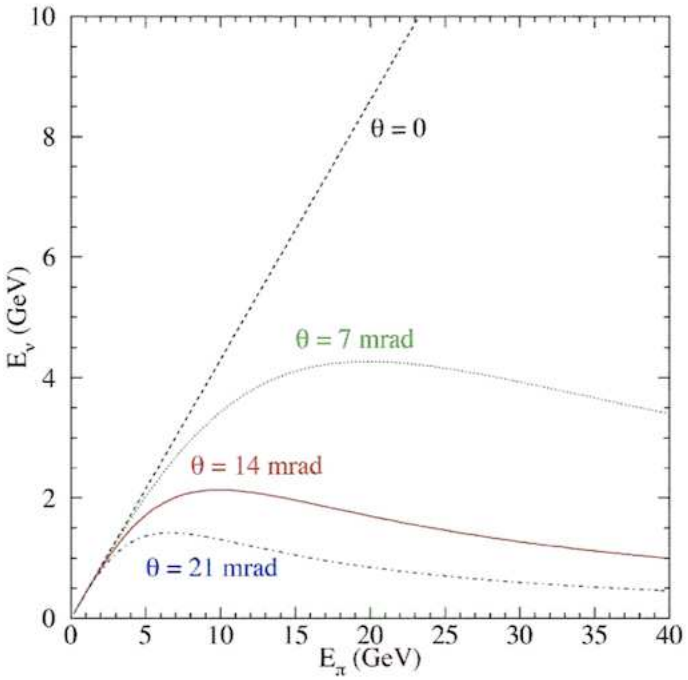

Figure 3.1: Plot of neutrino energy as a function of initial pion energy at different angles with respect to the beam axis. Image taken from [12].

$$E_\nu = \frac{0.43 E_\pi}{1 + \gamma^2 \theta^2} \tag{3.4}$$

where θ is the angle between the pion direction and neutrino direction. The result for kaons is identical within a factor, where 0.96 would be swapped for 0.43. This expression can be plotted for various angles as shown in Figure 3.1. For an angle of 14 mrad-off axis, the neutrino energy does not strongly depend on the initial pion energy. Although this does not quite produce a monoenergetic beam of neutrinos, it does narrow the neutrino beam energy spectrum significantly which reduces the effects of backgrounds in detector measurements. One example of such a background is NC events where the outgoing lepton is a neutrino, an "invisible" energy within the detector. The resulting neutrino carries much of the event energy away—this causes the visible energies in the detector to be lower than it should be. By having a narrow beam from the off-axis configuration these events are pushed out, reducing their contribution to the background.

3.3 Near and Far Detectors

Both the near and far detector are functionally identical and thus share a similar structure. Ultimately, the detectors are a specific arrangement of PVC plastic cells filled with liquid scintillator. One such cell is shown in Figure 3.2. The PVC cells are rectangular, rigid cells with dimensions of 3.9 cm wide, 6 cm deep, and 15.5 m long. Each PVC cell is filled with liquid scintillator made up of primarily mineral oil with 4.1% pseudocumene as the scintillant. Moreover, each cell has a looped wavelength-shifting fiber—the fiber is twice the length of the cell and looped at the bottom to route captured scintillation light to one end of the cell. From this end, the fiber directs the light to one pixel on an avalanche photodetector, which then converts the light to an electronic signal. This photodetector is known as the Avalanche Photodiode (APD), which is a semiconducting photodiode that exploits the photoelectric effect. When the light from the wavelength-shifting fibers reach the pixel, it is absorbed and generates electron-hole pairs. An applied electric field allows the electrons to propagate—the field is also sufficiently high which allows for an avalanche multiplication of electrons.

To create a signal, a neutrino would strike an atom in the scintillator which would excite the scintillant. This excited atom then returns back to the ground state, releasing UV light, which is then captured by the wavelength-shifting fibers. To ensure the light remains within the PVC cell, the cell itself is coated in a few millimeter thick layer of highly reflective titanium dioxide.

To arrange these cells within each detector, 32 PVC cells are installed side-by-side to form a plane of cells called an extrusion module. Multiple extrusion modules can be combined to form a larger plane. Several larger planes are then layered together where each layer alternates between a horizontal and vertical orientation of the cells as seen in Figure 3.3. These alternating layers create perpendicular planes of readout which allows for three-dimensional reconstruction of particle tracks. The ND consists of 496 32-cell extrusions while the FD has 12,036 extrusions.

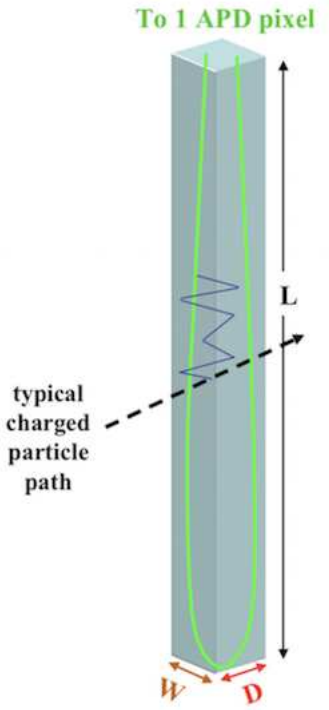

Figure 3.2: Depiction of PVC plastic cell in NOνA detector. Variables W, D, and L denote width, depth, and length, respectively. Each PVC cell is filled with liquid scintillator and contains a loop of wave-shifting fiber (bright green line). Image taken from [12].

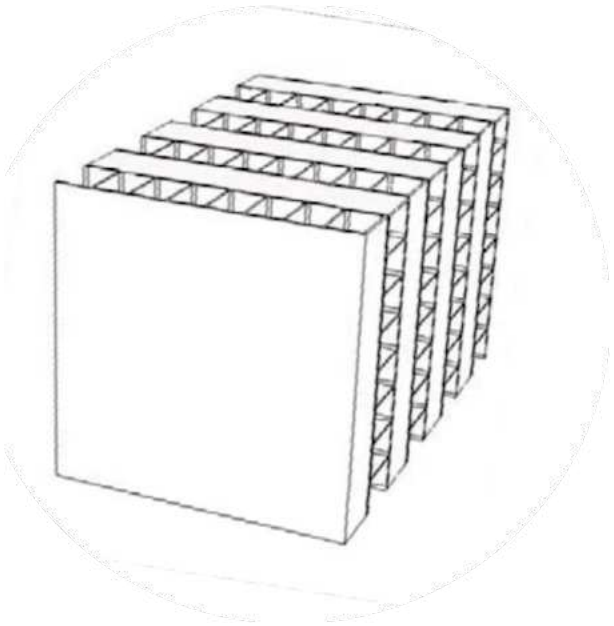

Figure 3.3: Representation of alternating vertical and horizontal layers within the NOνA detector. Image taken from [12].

3.4 Data Acquisition System

Each detector consists of over 368,000 APD channels to be analyzed and archived. To process this immense amount of data, NOνA has incorporated a data acquisition system (DAQ), which continuously collects and timestamps charge and time data from the APDs. An additional feature of the DAQ is to serve as a buffer stage for data, where it is determined to be recorded or rejected. What dictates "useful" data is determined by data-driven triggers (DDT), whose main function is to filter through the raw data stored in the DAQ and identify events. The DDT does this through the use of software filters. Some triggers use what is known as a Hough transform algorithm, which is an algorithm used to find vertices in the detector. The Hough transform analyzes the points or pixels of a two-dimensional image and identifies major lines or features [21]. Once an interesting event is found, a module broadcasts this decision to a global trigger system that alerts the system to permanently store the event(s). The primary purpose of the DDT is to find a class of non-beam event topologies useful for detector calibration, or to search for exotic physics such as supernova neutrinos.

Chapter 4

NOνA Software

A general outline of the NOνA software involves a simulation of detector events, the reconstruction of the simulated events, and an analysis post-reconstruction. A solid software package is a crucial element of any physics experiment as it allows for: the testing of hypotheses prior to detector construction, the optimization of detector design, the analysis and collection of data samples, and the computation of possible systematic errors [17]. It is thus important to develop a package that is robust and comprehensive to accomplish these goals, yet still efficient—NOνA does this by stringing together a few independent Monte Carlo (MC) generators as opposed to having just one. NOνA's event simulation consists of four main components: the beam simulator, the GENIE event generator [17], Geant4 [20], and reconstruction. First, the beam simulator creates neutrinos as described by the NuMI beam parameters. GENIE is then used to take the neutrino beam and simulate each neutrino's interaction in a detector, including secondary particles produced from the interactions. From there, the Geant4 package propagates the secondary particles and simulates energy deposition mechanisms, stores events and tracks, and offers a visualization tool of particle trajectories.

This chapter details each component that goes into the NOνA software including the beam simulator, GENIE, Geant4, reconstruction, and detector calibration techniques.

4.1 Neutrino Beam Simulation

The first step to simulating events in NOνA is to generate the incoming neutrino beam. This is done using two MC generators: FLUKA and Geant4. The purpose of the FLUKA generator is to simulate the neutrino beam production process described in the previous chapter. This includes taking the 120 GeV proton beam, modeling the interaction of this beam with the graphite target, the effects of the focusing horns, and determining the energy spectrum and flavor of the resulting neutrinos [29]. The Geant4 portion of the simulation is used to simulate the geometry of the

beamline [20]. These resulting neutrinos along with information about their parentage are stored and then used as inputs to the next step of the simulation: GENIE.

4.2 GENIE

There are many ways neutrino events can be generated, but the NOνA software framework chooses three: GENIE, CORSIKA, and Single particle generation [18]. All three of these methods share a similar framework of an object-oriented, C++-based, MC program. Describing these methods broadly: GENIE is a neutrino interaction generator primarily used for NOνA particle interaction simulations; CORSIKA, which has recently replace a similar generator CRY, is a cosmic ray generator that generates events at sea level; Single creates predefined particles at given energies and directions in the detector. Each event generator produces a list of particles along with their respective 4-momenta and positions—this represents an "event" in the detector. The Single particle generation is used in this study, but as it is heavily based on GENIE, the processes behind the GENIE software will be described [17].

GENIE is responsible for simulating neutrino interactions and incorporating the energy-dependence of these interactions, from several MeV to several hundred GeV [17]. This is especially necessary for correctly simulating the physics following the incoming beam, as neutrino beams inherently have a spread in energy. Once the neutrino-nucleon interactions are simulated by GENIE, the code outputs a list of final state particles along with their respective kinematic parameters.

4.3 Geant4

The simulation does not end with GENIE—GENIE only simulates particle interactions, but not how these final-state particles propagate through the detector. This is the role of Geant4: to take the final-state particles from an event generator such as GENIE, and simulate the propagation of said particles through the detector materials.

Like GENIE, Geant4 incorporates object-oriented technology using C++. Geant4 takes the 4-vectors resulting from GENIE, applies a set of physics models to handle interactions of particles

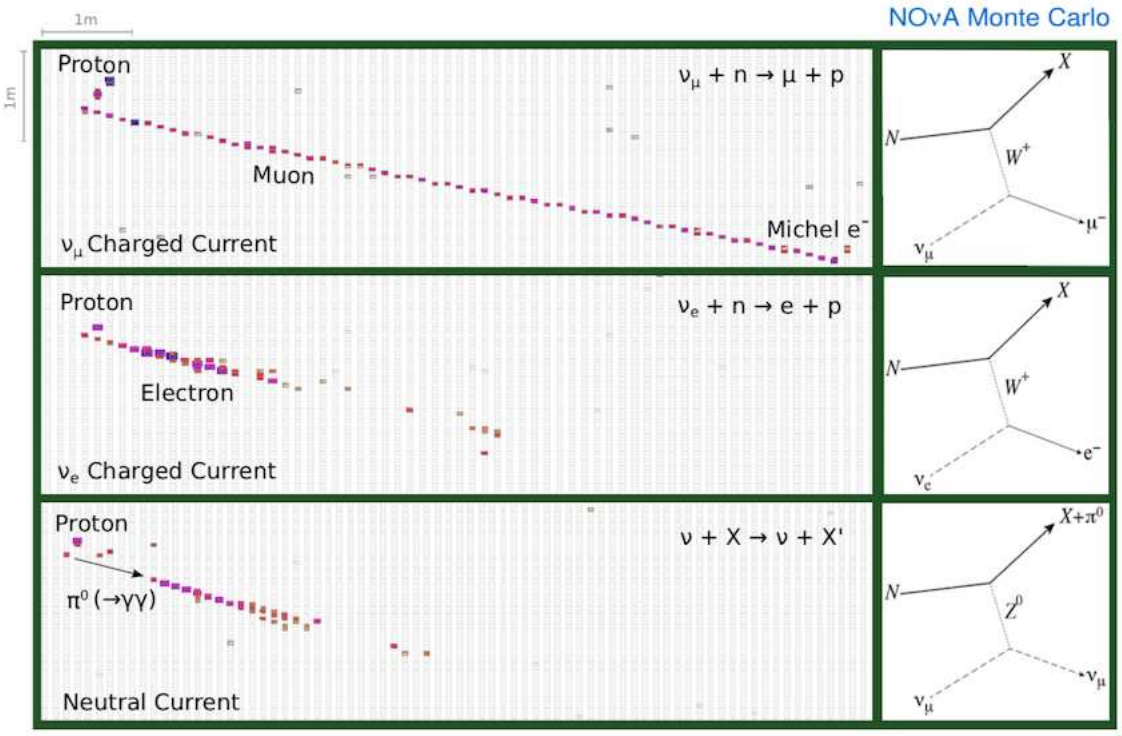

Figure 4.1: Simulated neutrino interactions using a 2.15 GeV beam. Each interaction can be deconstructed and assigned a fundamental interaction. Image taken from [21].

with matter, then outputs events as they would be seen in the detector. Some examples of simulated processes include: energy loss, secondary particle creation, scattering mechanisms, decay products, materials involved, and electromagnetic interactions [20]. An event display result after using Geant4 can be seen in Figure 4.1. Each colored track in the display can be interpreted as a string of energy deposits.

4.4 Reconstruction

Inside of the NOνA detectors, the events can be quite numerous—this is also reflected in the simulation results of Geant4. Thus, it is convenient to integrate a software capable of recognizing the topology of these events, while also rejecting background signals. This very process is known as "reconstruction" and for NOνA, the goal of reconstruction is to identify and generate topological objects like tracks and prongs.

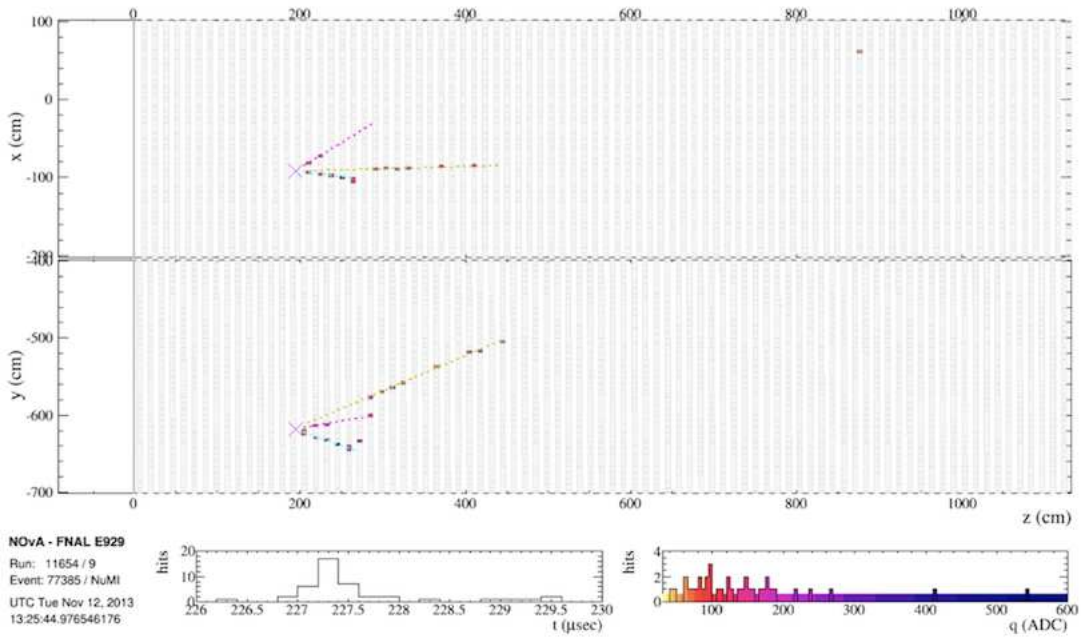

Figure 4.2: Event display of a neutrino event in the FD. Shows both 2D planes of the event. Image taken from [30].

In order to reconstruct an event in three-dimensions, NOνA combines two-dimensional readouts from the XZ planes and YZ planes. An event will consist of a series of charge deposits in both readout planes as seen in Figure 4.2. The reconstruction begins by clustering a collection of deposits based on time and space correlations into objects known as slices. Each slice then undergoes a Hough transform, to determines the three-dimensional vertex for the slice.

Once the vertex is determined, an algorithm is applied known as FuzzyK to reconstruct final-state particles into objects called prongs. A prong represents deposition from a single particle track or shower [21]. FuzzyK minimizes the distance among deposits in each view of the detector, in order to group the deposits into clusters which becomes a 2D prong. To then create a 3D prong, FuzzyK has to match 2D prongs from each view. This is achieve by calculating the cumulative energy fraction along prong length, creating energy profiles of the 2D prongs. The progression of the energy profile in one plane view is then compared to all possible profiles in the other plane. Those with similar profiles are matched and combined into a 3D prong. Not all 2D prongs are

matched in the process, so two distinct branches of data are defined: 3D prongs which represent matched pairs and 2D prongs which represent unmatched prongs.

Finally, the kinematic variables resulting from the 3D prong reconstruction are fed into a neural net known as the convolutional neural network (CNN) to determine the likeness of the event with a true ν_e CC interaction. If the interaction is interpreted to be ν_e CC, the relevant parameters of the interaction are stored. Other classifiers can be used for event identification, such as a Boosted Decision Tree (BDT), which takes input parameters and splits input data recursively based on those features [33].

4.5 Energy Calibration

A final note on the NOνA software is that it incorporates a calibration procedure for each cell within the detector. Calibration is done in two phases: a relative calibration to account for photon attenuation as it travels from one end of the cell to the APD; and an absolute calibration to convert the analog-to-digital signal (ADC), or charge, into units of energy in GeV. To assign energy values to an ADC value, standard candles with well-defined energy depositions are used. In particular, NOνA uses cosmic muons because their energy deposition is nearly uniform and flat along their trajectory [34].

Chapter 5

Single-Particle Simulation and Results

The goal of this analysis is to study the signatures of simulated neutron interactions in the NOνA near detector to develop a better understanding of how neutron interactions can be studied in the detector. To achieve this, mono-energetic neutrons incident on the ND were simulated using a single-particle generator. The generator used the standard MC described in the previous chapter. A study was performed to find the minimum neutron energy required to result in a reconstructed prong. Also undertaken was a study of the possibility of using charge deposits to identify neutrons in the detector. These results were then used to rationalize whether or not a D-T neutron source could feasibly be used as a neutron source in the ND.

This chapter discusses the simulation used for this study and the analysis of the simulated samples. Also included is a discussion on the feasibility of using a D-T source.

5.1 Event Generation

A beam of mono-energetic neutrons was simulated particle-by-particle using the NOνA software framework. This required the provision of a set of particle parameters such as: particle type, momentum in GeV, vertex location, and initial angle of incidence. The neutron momenta studied ranged from 100 MeV to 1 GeV, in increments of 100 MeV. An additional momentum of 162 MeV was also included, as this corresponded to the 14.1 MeV kinetic energy neutron produced from D-T fusion. It is more conventional to describe a particle's kinetic energy as opposed to its momentum; thus, this range was converted in terms of kinetic energy, which is detailed in Table 5.1. Relativistic corrections needed to be taken into account, so the kinetic energy was calculated using

$$KE = \sqrt{p^2c^2 + m^2c^4} - mc^2 \tag{5.1}$$

Momentum to Kinetic Energy Conversion		
Momentum	pc	Kinetic Energy
100 MeV/c	100 MeV	5 MeV
162 MeV/c	162 MeV	14.1 MeV
200 MeV/c	200 MeV	21 MeV
300 MeV/c	300 MeV	47 MeV
400 MeV/c	400 MeV	85 MeV
500 MeV/c	500 MeV	125 MeV
600 MeV/c	600 MeV	175 MeV
700 MeV/c	700 MeV	232 MeV
800 MeV/c	800 MeV	294 MeV
900 MeV/c	900 MeV	361 MeV
1000 MeV/c	1000 MeV	432 MeV

Table 5.1: Table converting the momenta of interest into kinetic energy in units of MeV. Relativistic corrections were considered as pc exceeded 10% of the neutron rest mass of 938 MeV/c^2 for most values considered.

To keep the neutron energy effectively mono-energetic, the variation in momentum was defined to be arbitrarily small at $\pm$100 eV/c. The vertex of each neutron was positioned randomly at the face of the ND. The angle of incidence was defined such that the neutron's momentum was perpendicular to the face plane. Finally, each simulation was performed twice: once using a standard setting, in which simulated detector noise was added to events; and a second time without noise.

Each simulation consisted of 10,000 neutrons to provide sufficient data, while keeping computation time reasonably low. The result of this simulation was a file containing event positions and momenta, as described in the Geant4 section. The events were then reconstructed into objects like prongs and tracks that were used in this analysis.

Variables resulting from the reconstruction were examined. These included number of 2D and 3D prongs per event. These variables were then plotted against neutron energy. Another product of reconstruction was files containing charge deposits information, or energy depositions within the detector. Charge deposits were extracted and summarized to probe lower energy regimes.

5.2 Prong Production

A study of the number of reconstructed prongs was performed. The efficiency of prong production was examined as a function of incident neutron momentum, or kinetic energy. Efficiency or prong production was defined to be the number of events that had 2D or 3D prongs divided by the total number of neutron events simulated. An event represented the full propagation of a neutron and its interactions within the detector, before the next neutron was simulated. Both 2D and 3D prongs are mutually exclusive—2D prongs are unmatched prongs from the reconstruction process while 3D prongs are matched. A plot of both prong efficiencies can be seen in Figures 5.1 and 5.2.

Prong production in the ND did not appear to dramatically increase until about 85 MeV kinetic energy for both 2D and 3D prongs, which corresponded to a neutron momentum of 400 MeV. This production threshold was quite a bit above the D-T source energy of 14.1 MeV—in fact, for 10,000 neutrons simulated, the number of non-zero 2D and 3D prongs for the D-T source was exactly zero.

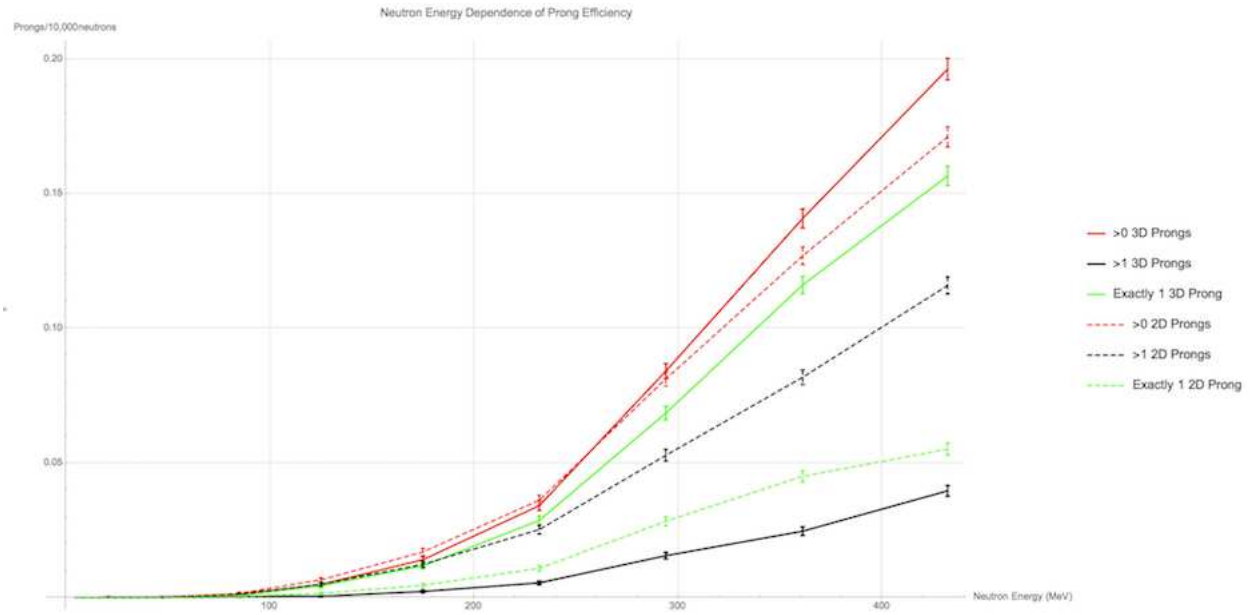

Figure 5.1: Energy dependence of 3D and 2D prong production for a beam of neutrons. The solid line represents 3D prongs and dashed for 2D prongs. Error bars were calculated using margin of error.

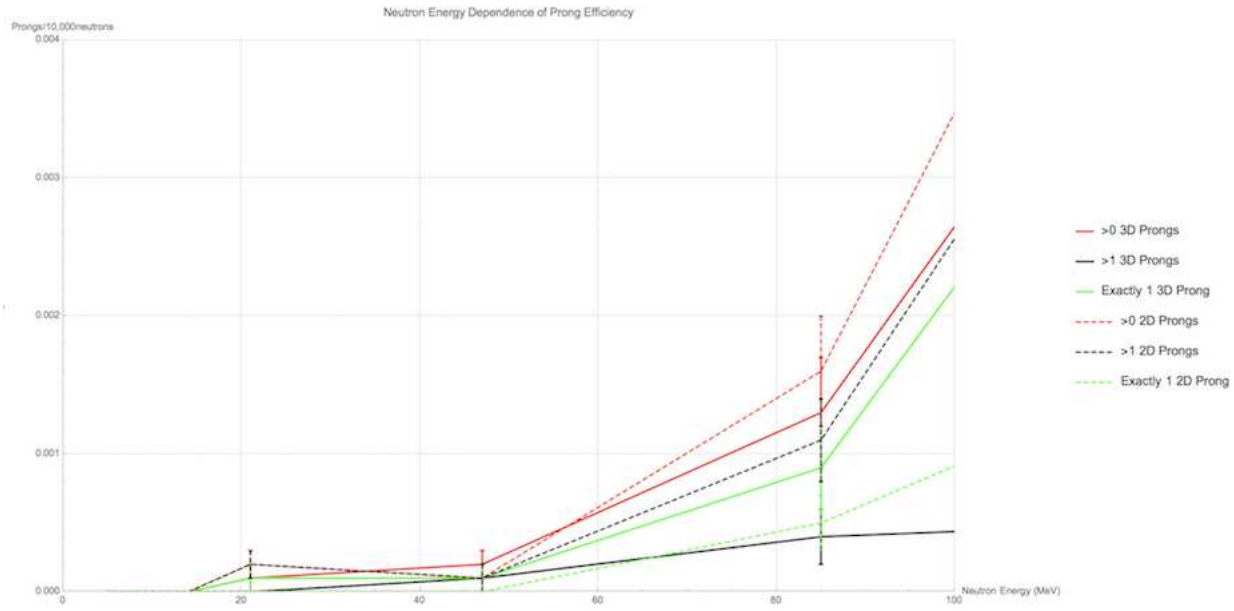

Figure 5.2: Similar plot to 5.1, but zoomed in at the lower energies to identify the "turn on" energy. Error bars were calculated using margin of error.

5.3 Charge Deposits

Since the prong production efficiency for energies less than 85 MeV was very low, another simulation product was analyzed to see if lower energy neutrons have signatures that can be distinguished from noise. Charge deposits, which are quantified by ADC values, were studied to probe the lower energy neutron energies. As described in the calibration section of Chapter 4, the ADC value is a proxy for energy, so charge deposits can be interpreted as energy deposits. Visually, these deposits represented colored blocks in the event displays as shown in Figures 5.3 and 5.4. The color of the block is indicative of the magnitude of the ADC of the deposit. Charge deposit information was analyzed in two ways: the average number of deposits per event as a function of neutron energy; and total ADC distribution for each neutron energy. Charge deposits were compared for both standard and noiseless simulations. Error bars for plots that compared averages was calculated using a standard error procedure

$$Standard\ Error = \frac{\sigma}{\sqrt{N}} \tag{5.2}$$

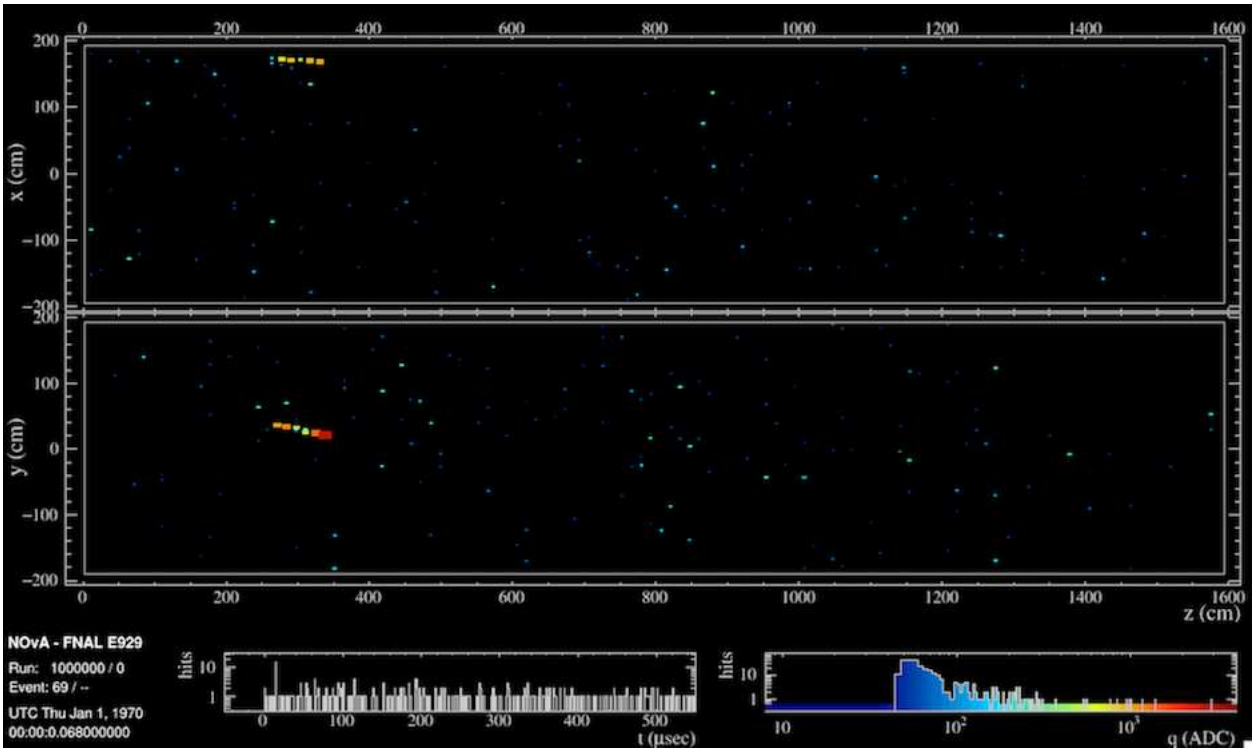

Figure 5.3: An event display including noise. The incident neutron had a momentum of 1 GeV/c, or 432 MeV kinetic energy.

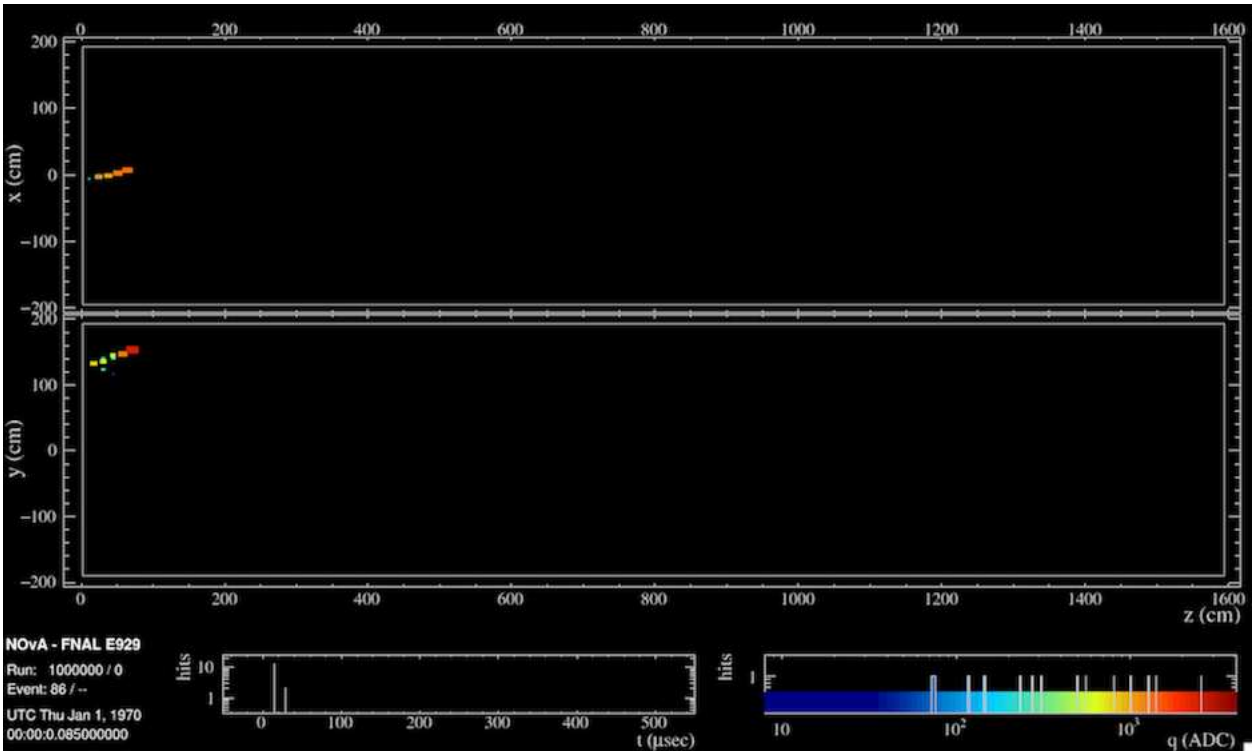

Figure 5.4: A noiseless event display. The incident neutron also had a momentum of 1 GeV/c, or 432 MeV kinetic energy.

where σ represents the standard deviation and N is the sample size of 10,000 events.

Plots of the average number of deposits as a function of neutron kinetic energy are shown in Figures 5.5 and 5.6. As would be expected, the number of deposits per event increased with incident neutron energy. Higher energy neutrons are kinematically capable of depositing more charge above the energy threshold of NOνA, which is around 6-8 MeV. At the D-T energy of 14.1 MeV, it appeared that charge deposits were produced, but it was not clear whether these deposits were above noise.

To see how the number of charge deposits compared to noise, histograms were produced looking at the magnitude of the charge for each deposit. Noiseless and with noise included in the simulations were compared for each energy. Characteristic plots are pictured in Figures 5.7 and 5.8. The remaining plots for various neutron energies can be found in Appendix A.

One defining feature of the noise-simulated histograms is the large number of deposits up until 300 ADC, where there is a sharp drop in values. This is due to the noise simulation being artificially cut off, as the noise distribution of the detector is largely below this value. As such, ADC values below 300 will be difficult to distinguish over noise. In order to use a D-T source, there would need to be a reasonable number of deposits above 300 ADC, which was not particularly convincing especially when compared to the 432 MeV source.

Before ruling the D-T source out completely, additional data was gathered at this 14.1 MeV energy. The simulation was run again at 100,000 neutrons and one million neutrons. Both prongs and ADC histograms were analyzed.

The prong production for 100,000 neutron at the D-T energy was quite small—only six 3D prongs and 18 2D prongs total out of 100,000 events. For the one million events, 25 3D prongs were present and 77 2D prongs. Due to this high level of inefficiency, charge deposits were instead analyzed. The average number of deposits was on par with that of the 10,000 neutron simulation. For 100,000 the average was 1.96 deposits per event for noiseless and 303.9 deposits per event for the noise simulation. For one million events the average deposits per event were 1.95 and 303.4 for

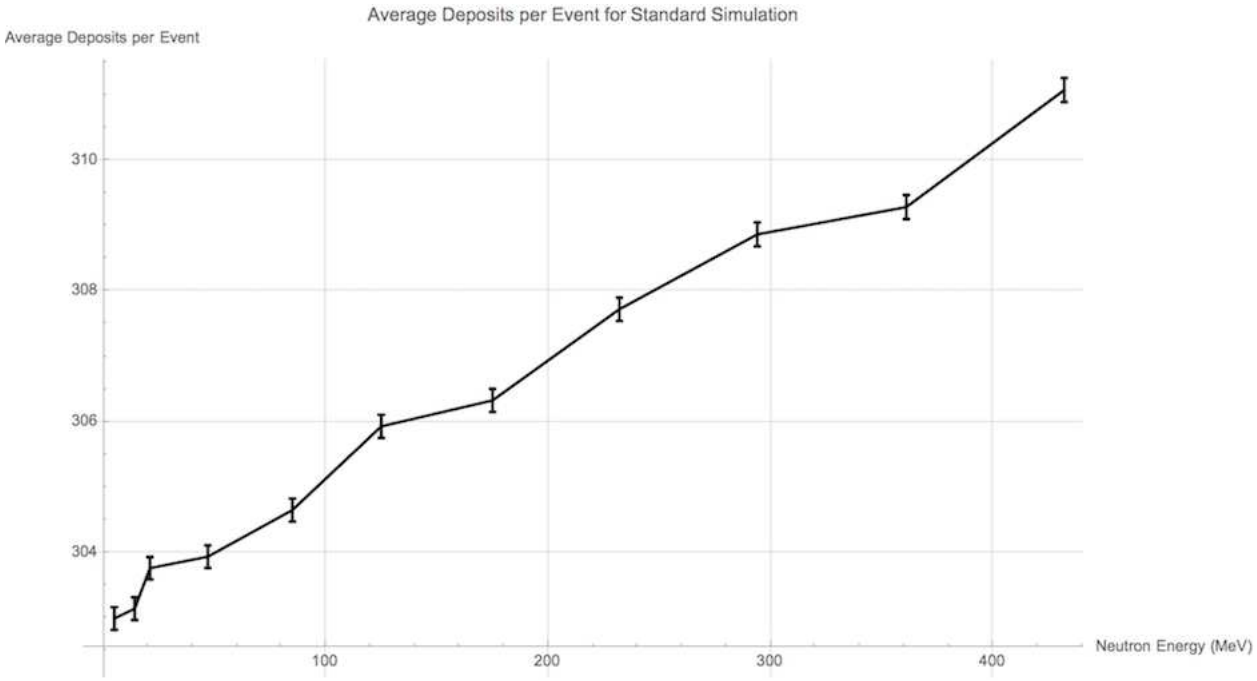

Figure 5.5: Average number of deposits per event as a function of neutron energy for the standard simulation. Includes error bars using the standard error formulation.

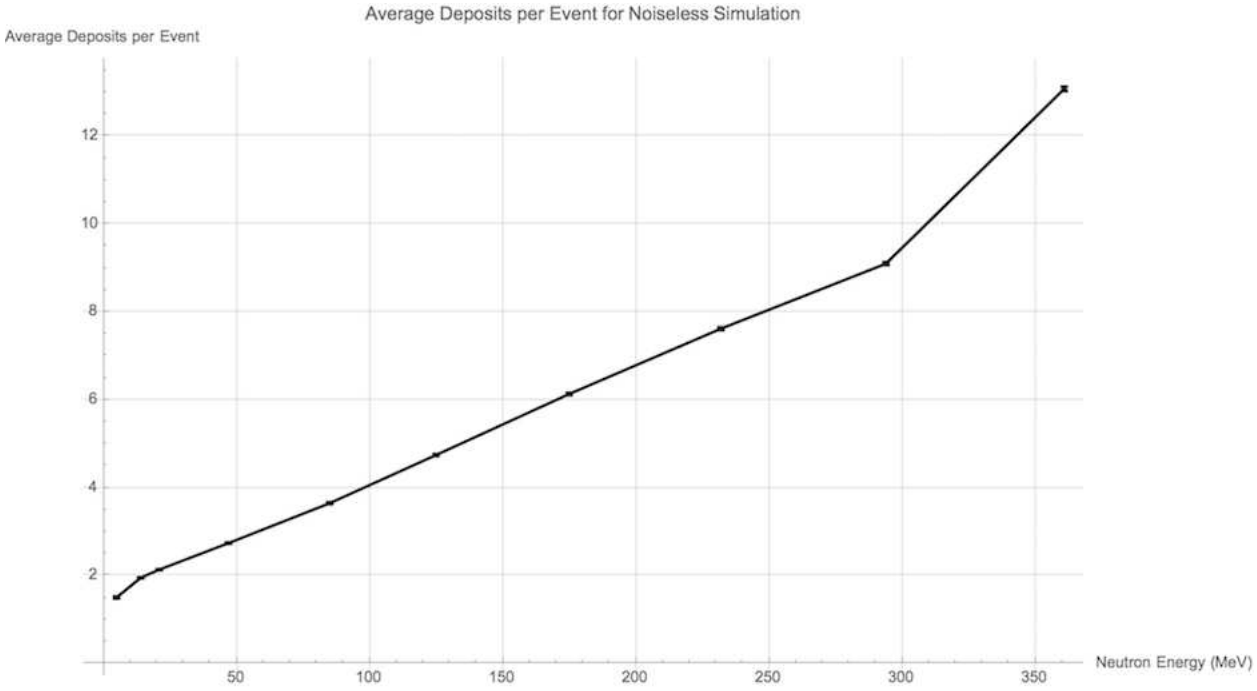

Figure 5.6: Average number of deposits per event as a function of neutron energy for the noiseless simulation. Includes error bars using the standard error formulation. Standard error here was very small, so the error bars are barely visible.

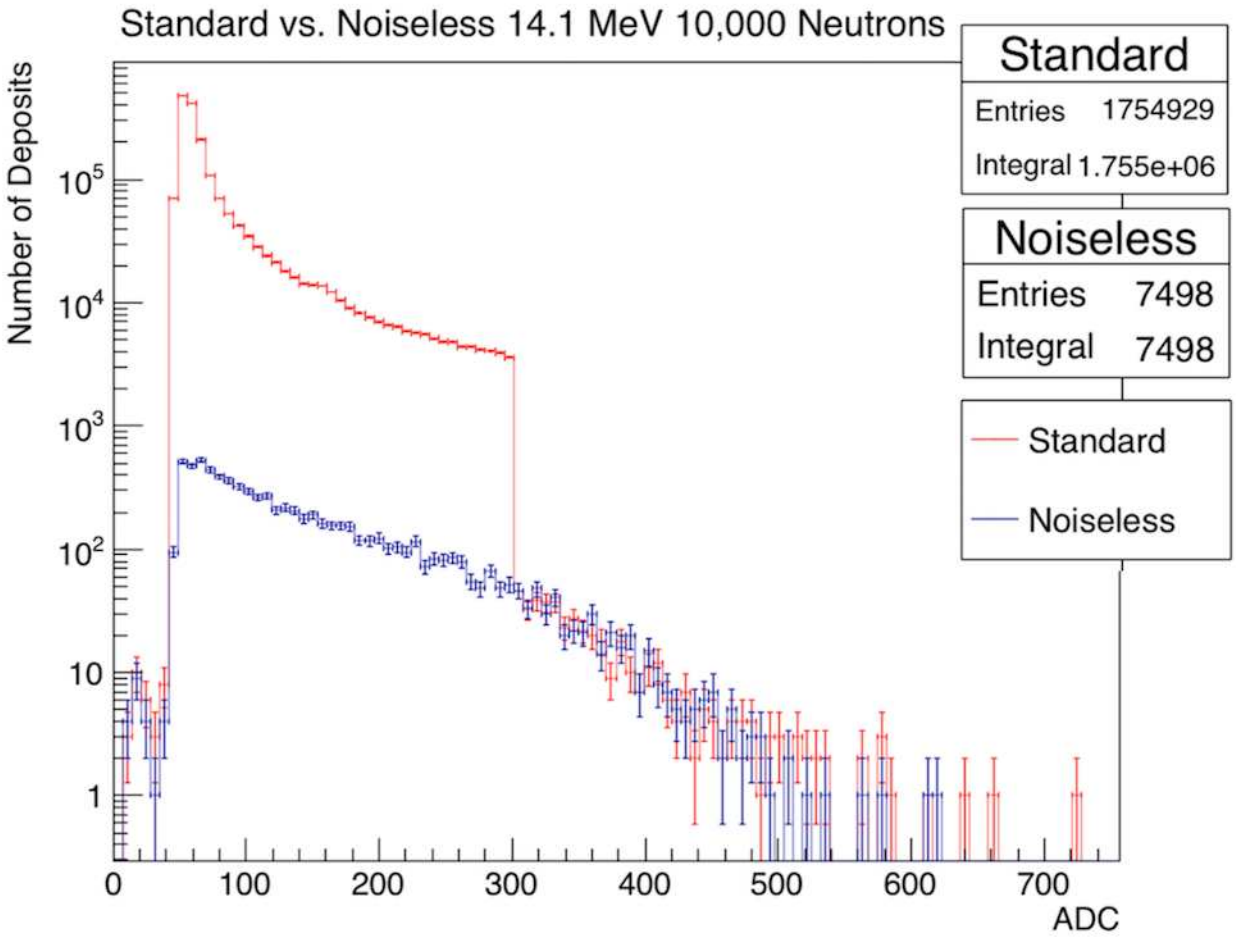

Figure 5.7: Semi-log plot of histogram comparing the charge per deposit for both standard and noiseless simulations at the D-T neutron energy of 14.1 MeV.

noiseless and with noise, respectively. As for the charge deposit distribution, histograms of ADC per deposit can be seen in Figures 5.9 and 5.10 for the 100,000 and one million neutrons.

Qualitatively, there appeared to be better data volume above the 300 ADC noise cut off. With high statistical values, a D-T source looks promising for studying lower energy mechanism of neutron kinematics within the ND.

5.4 Feasibility of Experimentation

From the analysis above, a D-T source requires a large sample size of neutrons to differentiate from noise; thus, a D-T device would need to output a significant number of neutrons. The neutron

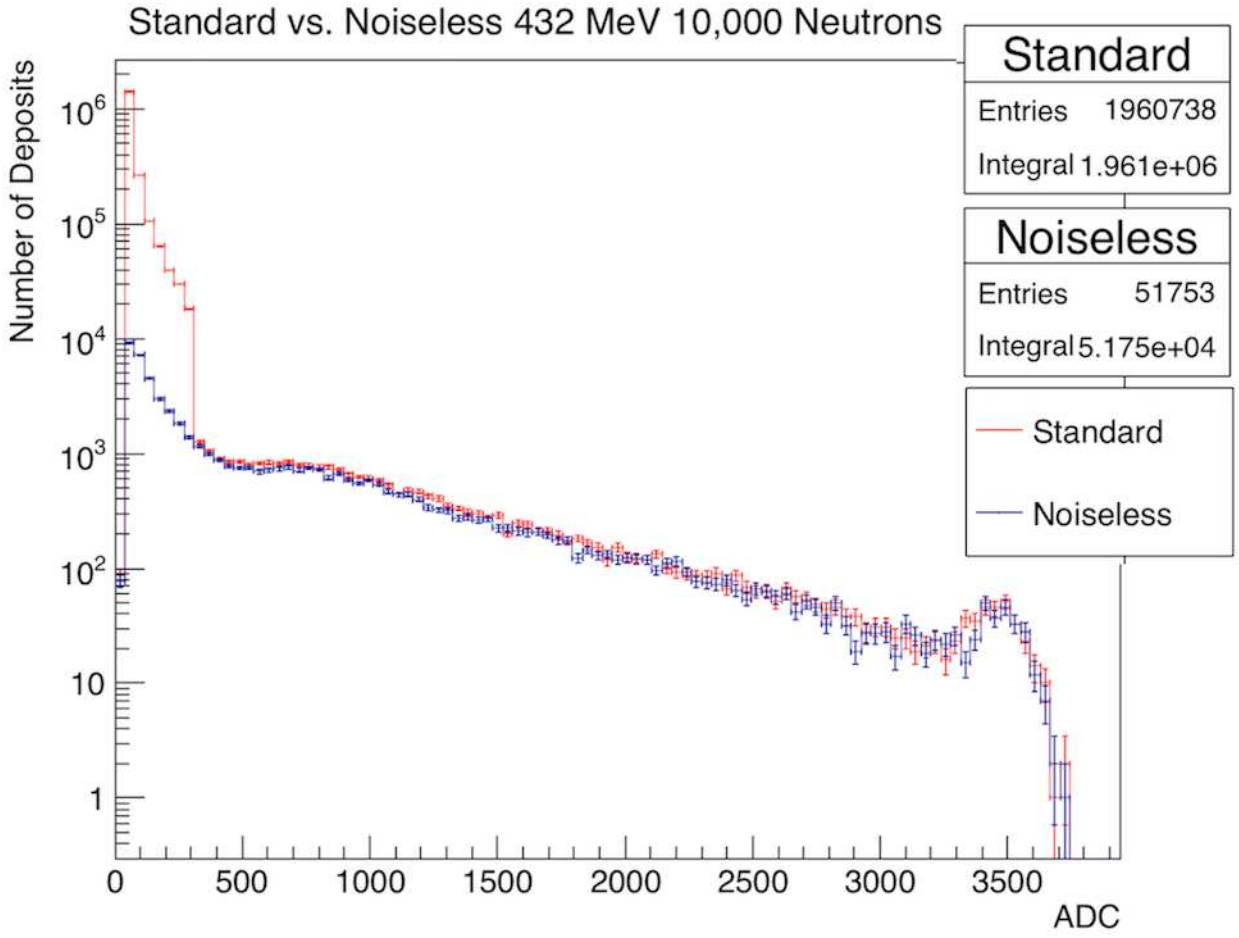

Figure 5.8: Semi-log plot histogram comparing the charge per deposit for both standard and noiseless simulations at the highest energy simulated of 432 MeV kinetic energy.

yield of various commercial devices is explored in Table 5.2. Given the neutron yield of around 10^8 neutrons per second of a modest generator, it appears that the necessary data can be obtained with current generator technologies; however, more research would need to be done to determine the data production capabilities of the source in greater depth. In principle, a D-T source could be used in the NOνA ND and produce measurable results.

Based on neutron cross sections for hydrogen and carbon, these deposits would correspond to elastic collisions, inelastic collisions with the emission of gamma radiation, or neutron capture with the emission of gamma radiation or an alpha particle. Energies for these mechanisms range from hundreds of keV to a few MeV. Given the energy resolution of the NOνA ND of only 6-8

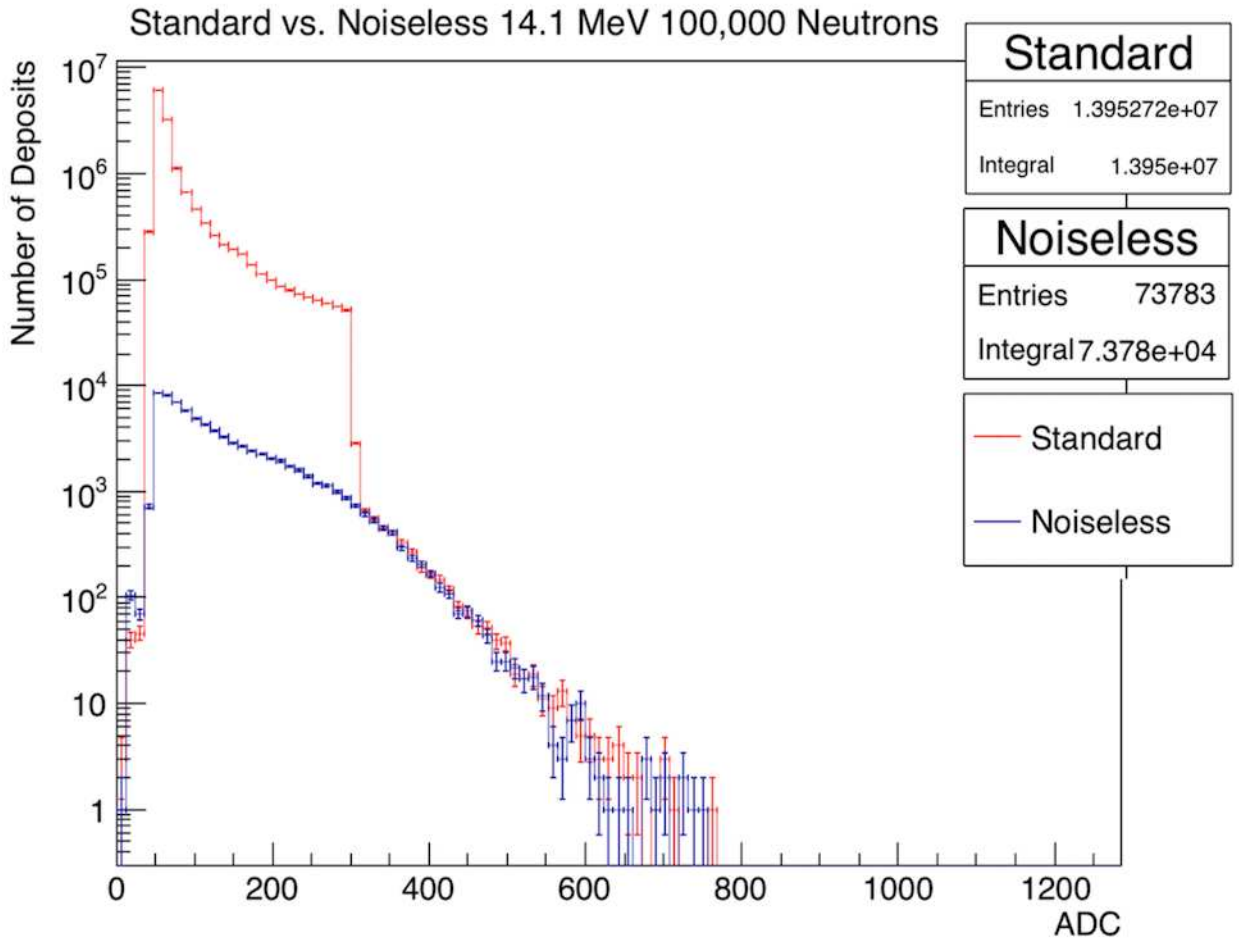

Figure 5.9: Semi-log plot histogram comparing the charge per deposit for both standard and noiseless simulations at 14.1 MeV. 100,000 neutrons were simulated.

MeV, only a narrow distribution of photon energies from inelestic collisions and neutron capture could be observed. Elastic collisions could also be observed, but these interactions would also be quite limited. Each collision would decrease the neutron's energy—being that the incident neutron energy is already close to threshold, only a handful of collisions would be visible in the detector.

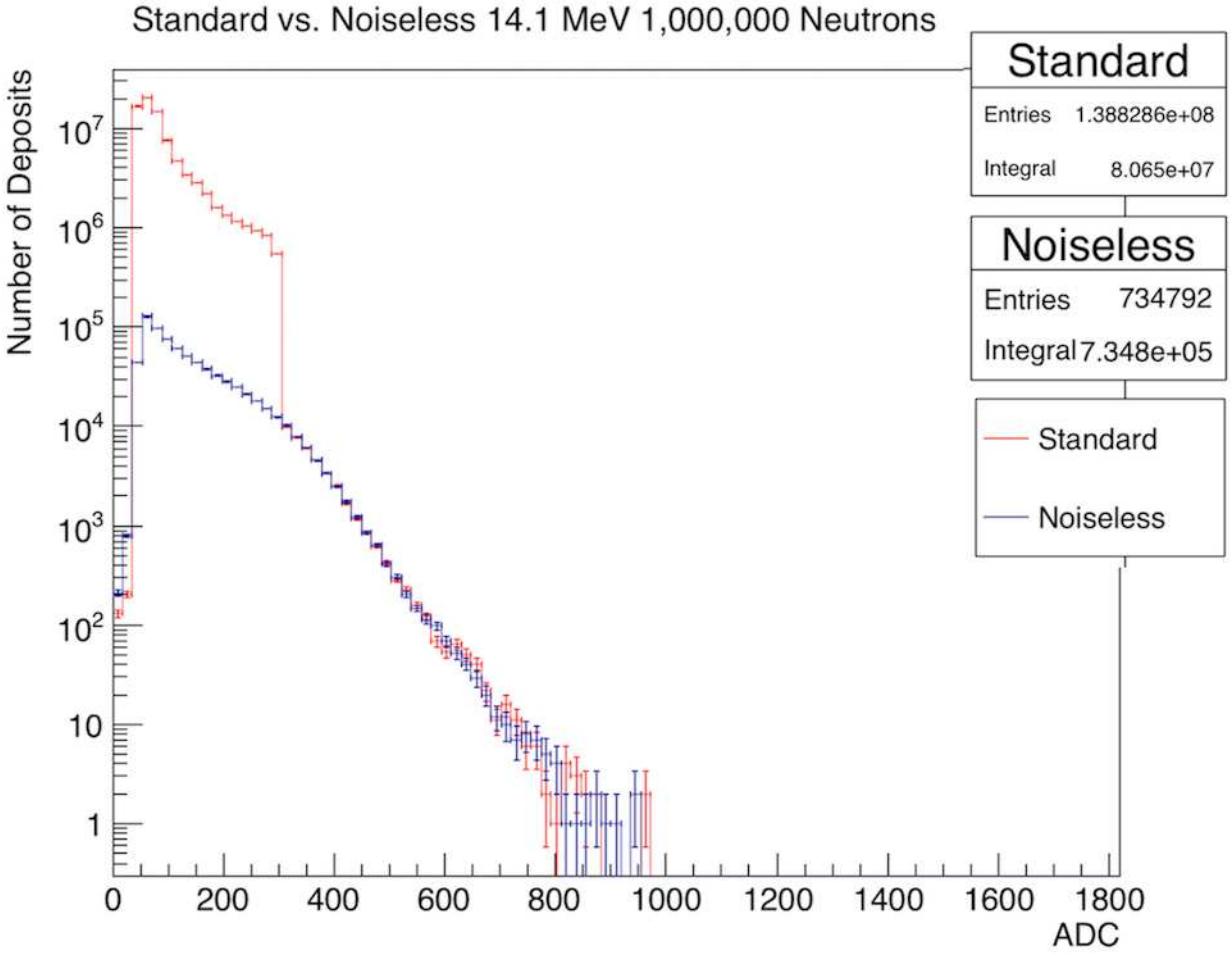

Figure 5.10: Semi-log plot histogram comparing the charge per deposit for both standard and noiseless simulations at 14.1 MeV. One million neutrons were simulated.

D-T Neutron Generators		
Model/Manufacturer	Size	Neutron Yield
Neutristor/Sandia National Labs	1.54 cm x 3.175 cm	10^4-10^5 n/s
miniGen/Thermo Scientific	20.3 cm x 25.4 cm x 10.8 cm	3*10^8 n/s
nGen 300/Starfire Industries	7.6 cm D x 46 cm L	5*10^8 n/s
DT110/Adelphi Technology	1 cm x 4 cm	10^{10} n/s
Alectryon300/Phoenix	Room Sized (4m)	10^{13} n/s

Table 5.2: Table looking at various neutron generator manufacturers. Size of the generator and neutron yields are compared.

Chapter 6

Conclusion

Understanding neutron kinematics within the NOνA ND is critical to fully understanding neutrino and antineutrino CCQE interactions. By constraining the cross section measurement of CCQE interactions, the NOνA experiment can be one step closer to lowering systematic uncertainties and achieving their physics goal of precise oscillation measurements. This thesis has presented the feasibility of studying neutron interactions within the NOνA ND, which was done by simulating mono-energetic single neutrons incident on the ND and analyzing prong production and charge deposits.

A possible D-T source was also considered, to see if experimentation was feasible. Given that the energy of D-T neutrons is only a factor of two above the 6-8 MeV threshold for the ND, many interaction mechanisms may be difficult to study. It can be possible to look at elastic scattering of the neutron within the detector; however, even this may be limited as the neutron would lose energy after each collision, reaching the detector threshold after only a few collision. If other neutron interactions want to be analyzed in the NOνA ND, a higher energy source needs to be considered, which would come with the trade-off of higher cost or having a nuclear reactor in the vicinity of the detector. Despite the limitations of using D-T source neutrons, probing this regime may be feasible with a high neutron volume source and with improved reconstruction and analysis tools.

Bibliography

[1] University of Liverpool, 80 years since discovery of the neutron (2012). Retrieved from https://phys.org/news/2012-06-years-discovery-neutron.html.

[2] D. Griffiths, *Introduction to Elementary Particles*, 1987.

[3] M. F. L'Annunziata, *Radioactivity Introduction and History*, 2007.

[4] D.A. Brown, M.B. Chadwick, *et al.*, "ENDF/B-VIII.0: The 8th Major Release of the Nuclear Reaction Data Library with CIELO-project Cross Sections, New Standards and Thermal Scattering Data", *Nuclear Data Sheets*, **1**48, pp. 1-142 (2018).

[5] M. Betancourt, Study of the Quasi-Elastic Scattering in the NOvA Detector Prototype, Ph.D Thesis, 2013.

[6] M. Judah, Measurement of the Inclusive Electron-Neutrino Charged-Current Cross Section in the NOvA Near Detector, Ph.D Thesis, 2019.

[7] *Standard Model of Particle Physics.* (2018). Retrieved from https://www.physik.uzh.ch/.

[8] P. Higgs, Phys. Rev. Lett. 13, 508 (1964).

[9] What's a neutrino? (n.d.). Retrieved from https://neutrinos.fnal.gov/whats-a-neutrino/.

[10] International Atomic Energy Agency, *Thermal Neutron Capture Gamma's (CapGam* https://www-nds.iaea.org/capgam/indexbyn.htmlx.

[11] A. Habig and the NOvA Collaboration, The NOvA Experiment. *Nuclear Physics B (Proceedings Supplements)*, vol. 229-232, pp. 460-460, 2012.

[12] D. S. Ayres, et al., The NOvA Technical Design Report, Tech. Rep. FERMILAB-DESIGN-2007-01, Fermilab (2007).

[13] How does NOvA work? (n.d.). Retrieved from https://novaexperiment.fnal.gov/how-does-nova-work/.

[14] D. S. Ayres, et al., NOvA Proposal to Build a 30 Kiloton Off-Axis Detector to Study Neutrino Oscillations in the Fermilab NuMI Beamline, 2005. Retrieved from https://arxiv.org/abs/hep-ex/0503053.

[15] K. E. Duffy, First Measurement of Neutrino and Antineutrino Oscillation at T2K, Ph.D Thesis, 2017.

[16] Y. Hayato, *Overview of neutrino-nucleus interactions (From an experimentalist's point of view)* [PowerPoint Slides]. https://indico.ihep.ac.cn/.

[17] C. Andreopoulos, A. Bell, D. Bhattacharya, F. Cavanna, J. Dobson, S. Dytman, H. Gallagher, P. Guzowski, R. Hatcher, P. Kehayias, A. Meregaglia, D. Naples, G. Pearce, A. Rubbia, M. Whalley and T. Yang, Nucl. Instrum. Meth. A **614**, 87-104 (2010) doi:10.1016/j.nima.2009.12.009 [arXiv:0905.2517 [hep-ph]].

[18] NOvA-ART Running NOvA Simulations. (n.d.). Retrieved from https://cdcvs.fnal.gov/redmine/projects/novaart/wiki/.

[19] The Use of Geant4 by FNAL Neutrino Experiments. (n.d.). Retrieved from https://web.fnal.gov/project/Geant4/SitePages/NuExptUseOfG4.aspx.

[20] S. Agostinelli *et al.* [GEANT4], Nucl. Instrum. Meth. A **506**, 250-303 (2003) doi:10.1016/S0168-9002(03)01368-8.

[21] M. Baird, J. Bian, M. Messier, E. Niner, D. Rocco, and K. Sachdev, "Event reconstruction techniques in NOvA," *Journal of Physics: Conference Series*, vol. 664, p. 072035, dec 2015.

[22] M Fischler *et al.* 2012 *J. Phys.: Conf. Ser.* **396** 012020.

[23] M. Aker, K. Altenmuller, M. Arenz, *et al.*, Phys. Rev. Lett. 123, 221802 (2019) doi:10.1103/PhysRevLett.123.221802.

[24] C. Jensen F. Aaserud, Controversy and consensus: nuclear beta decay 1911-1934. Birkhauser Verlag. (2000).

[25] E. Fermi, Z. Physik 88, 161 (1934).

[26] J. A. Formaggio and G. P. Zeller, Rev. Mod. Phys. 84, 1307 (2012).

[27] E. D. Niner, "Observation of Electron Neutrino Appearance in the NuMI Beam with the NOvA Experiment," Ph.D. Thesis, FERMILAB-THESIS-2015-16.

[28] A Aurisano, *et al.* J. Phys.: Conf. Ser. 664 072002 (2015).

[29] G. Battistoni, F. Cerutti, A. Fasso, A. Ferrari, S. Muraro, J. Ranft, S. Roesler, and P. R. Sala, AIP Conference Proceedings 896, 31 (2007).

[30] S. Yu, arXiv:1910.06953 [physics.ins-det].

[31] T. P. Lou, "Compact D-D/D-T Neutron Generators and Their Applications," Ph.D. Thesis, 2003.

[32] M. Baird, *Event Display Tutorial* [PowerPoint Slides]. `https://nova-docdb.fnal.gov/`.

[33] K. Woodruff, *Introduction to boosted decision trees* [PowerPoint Slides]. `https://indico.fnal.gov/`.

[34] Z. Jelinkova, "Study of neutrino properties using NOvA detector," Masters Thesis, 2017.

[35] G. Jennings, C. Sanzeni, and D.R. Winn, arXiv:1308.0327.

[36] Thermo Scientific. *Thermo Scientific miniGen Neutron Generator* `https://www.thermofisher.com`.

[37] Starfire Industries. *nGen-300 FOR SHARP PULSED NEUTRONS*

http://www.starfireindustries.com/.

[38] Adelphi Technology. *DT110-14 MeV Neutron Generator*

http://adelphitech.com/products/dt109-dt110.html.

[39] Phoenix. *Alectryon High Flux Neutron Generator*

https://phoenixwi.com/neutron-generators/alectryon/.

Appendix A

ADC per Deposit Histograms

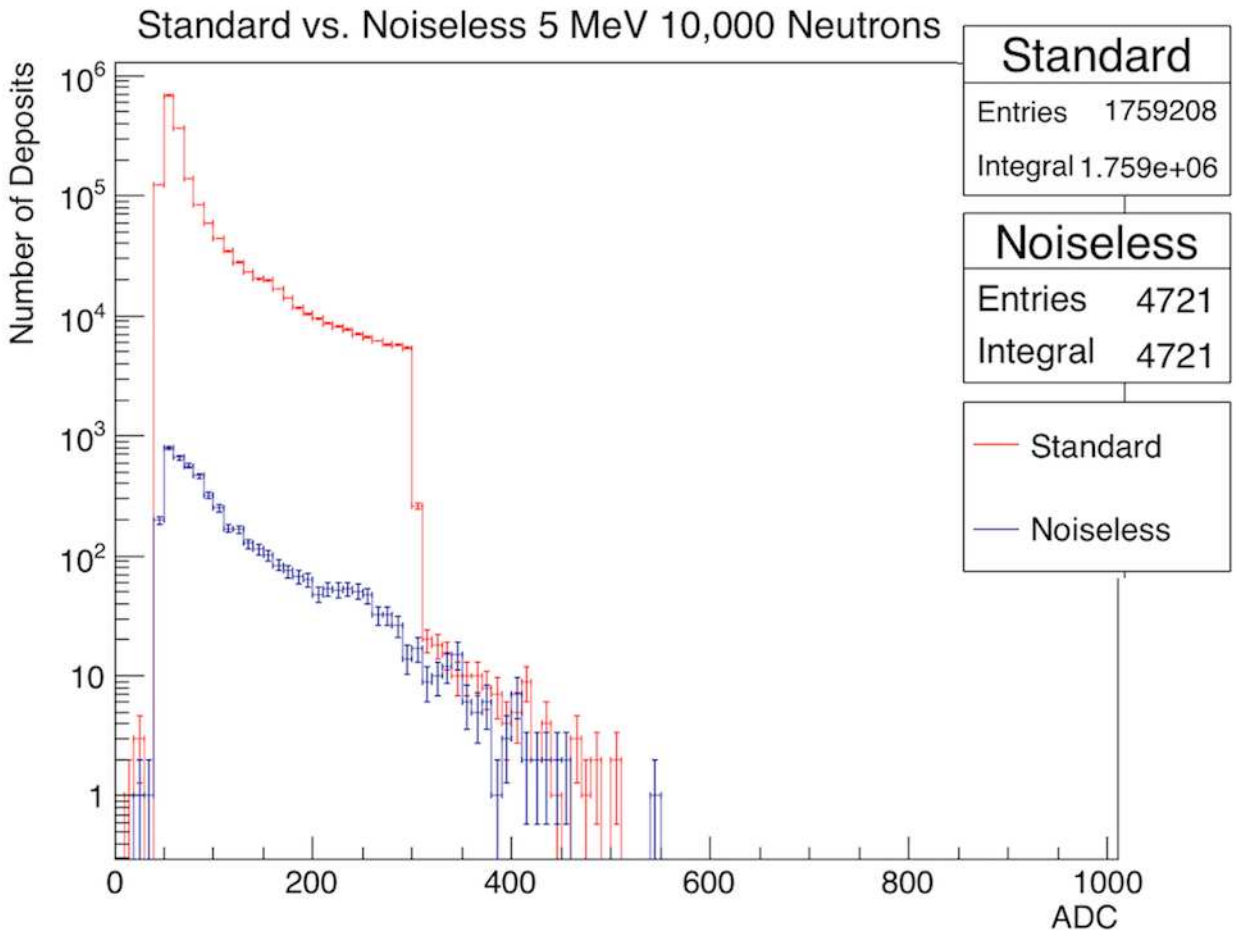

Figure A.1: Standard vs noiseless ADC per charge deposit for 10,000 neutron events at 5 MeV kinetic energy. On a semi-log plot.

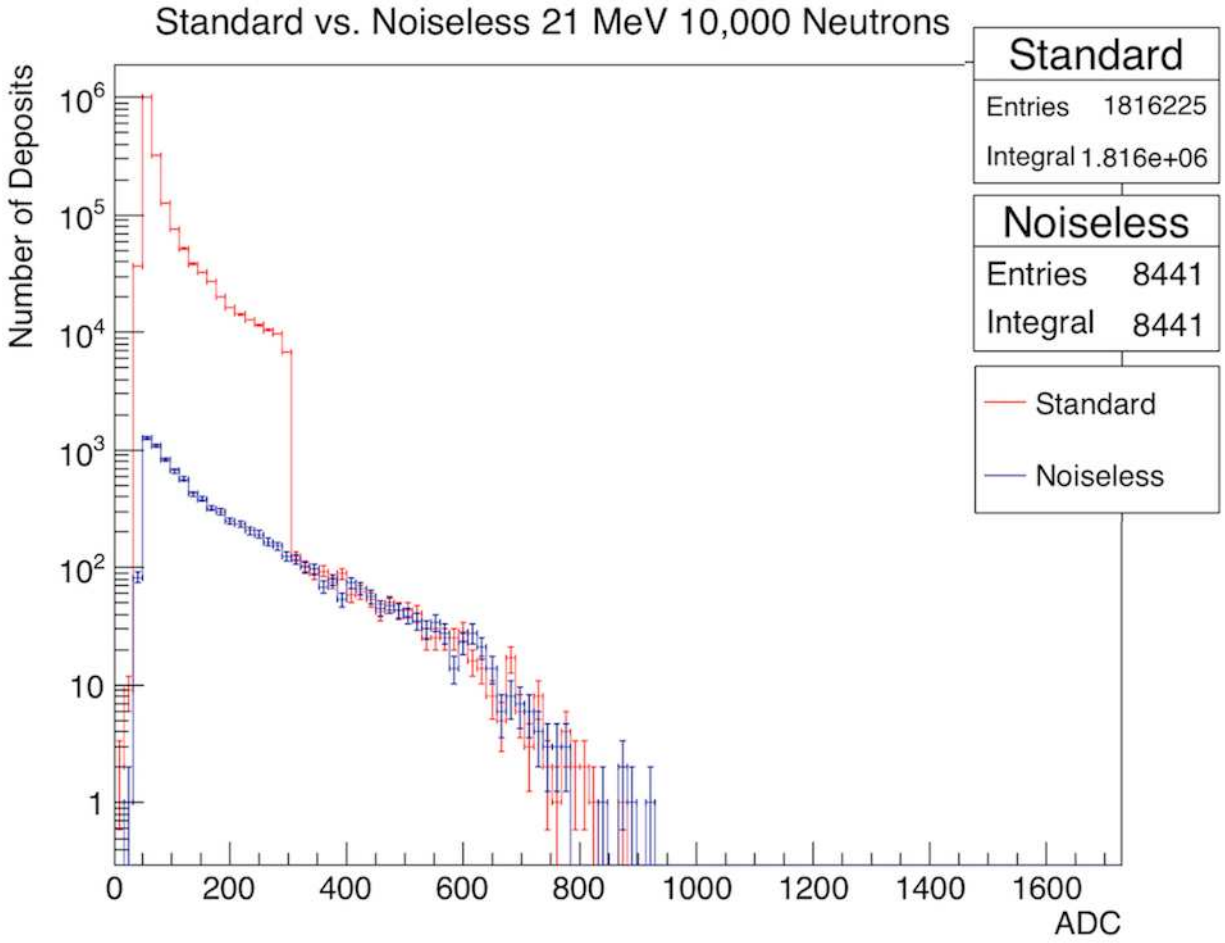

Figure A.2: Standard vs noiseless ADC per charge deposit for 10,000 neutron events at 21 MeV kinetic energy. On a semi-log plot.

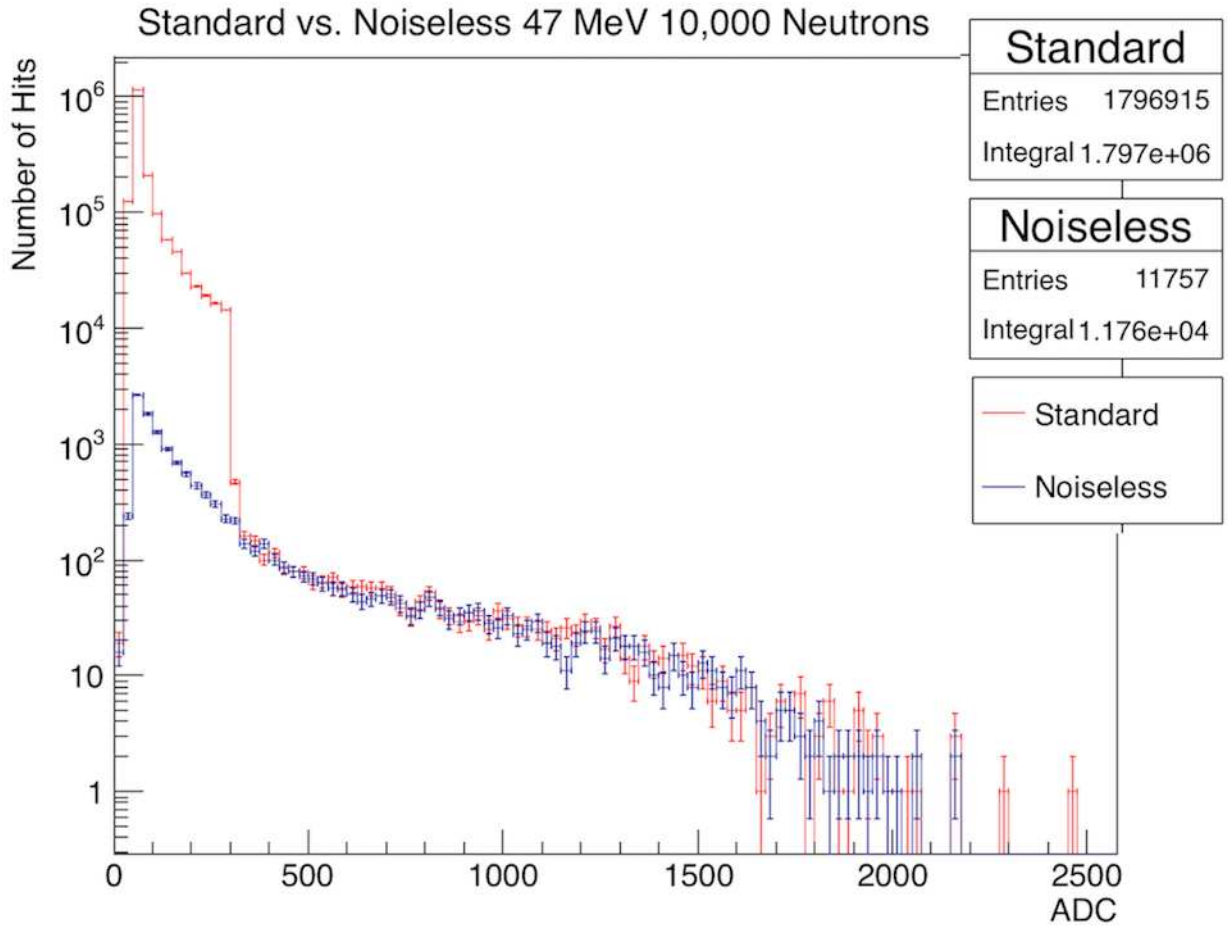

Figure A.3: Standard vs noiseless ADC per charge deposit for 10,000 neutron events at 47 MeV kinetic energy. On a semi-log plot.

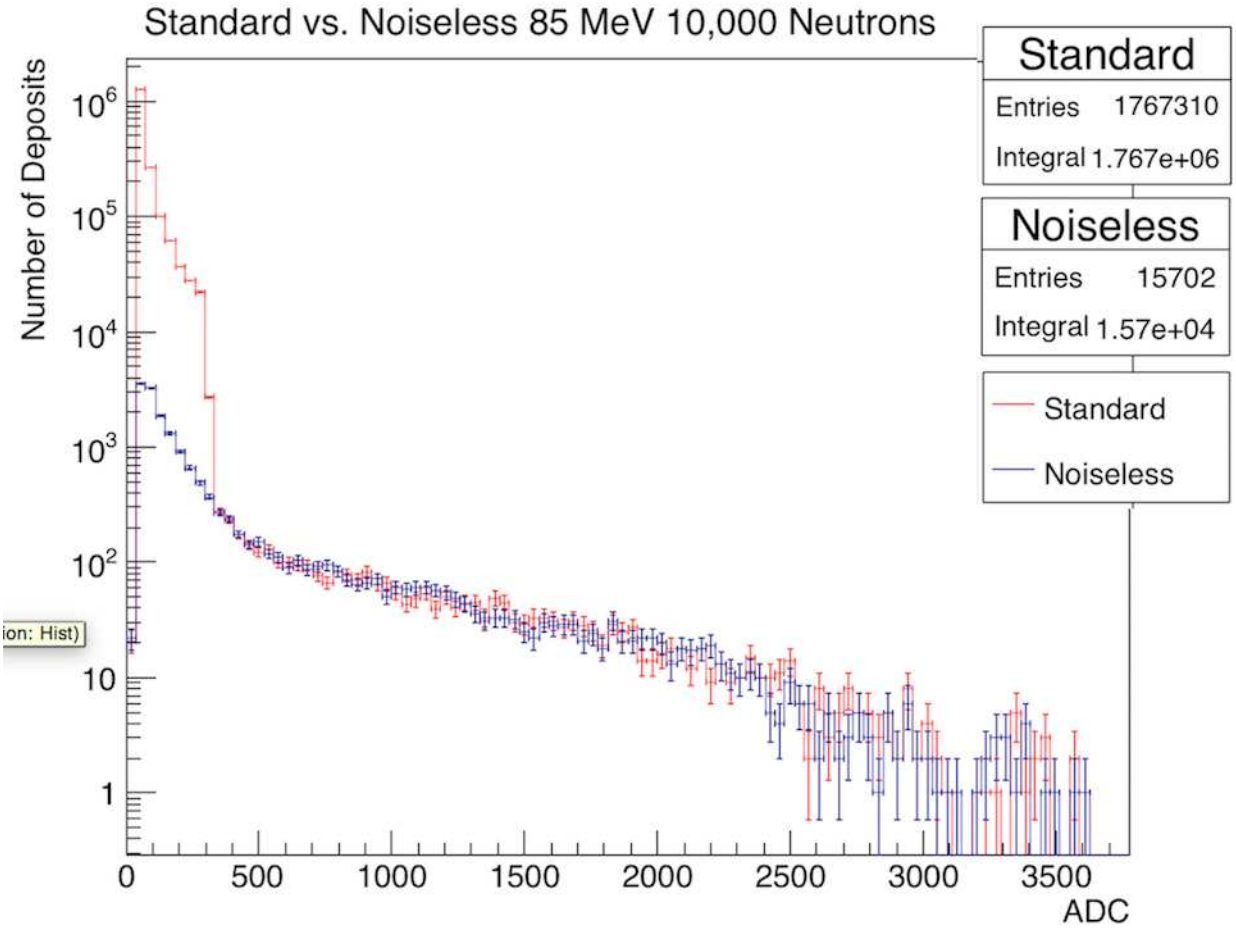

Figure A.4: Standard vs noiseless ADC per charge deposit for 10,000 neutron events at 85 MeV kinetic energy. On a semi-log plot.

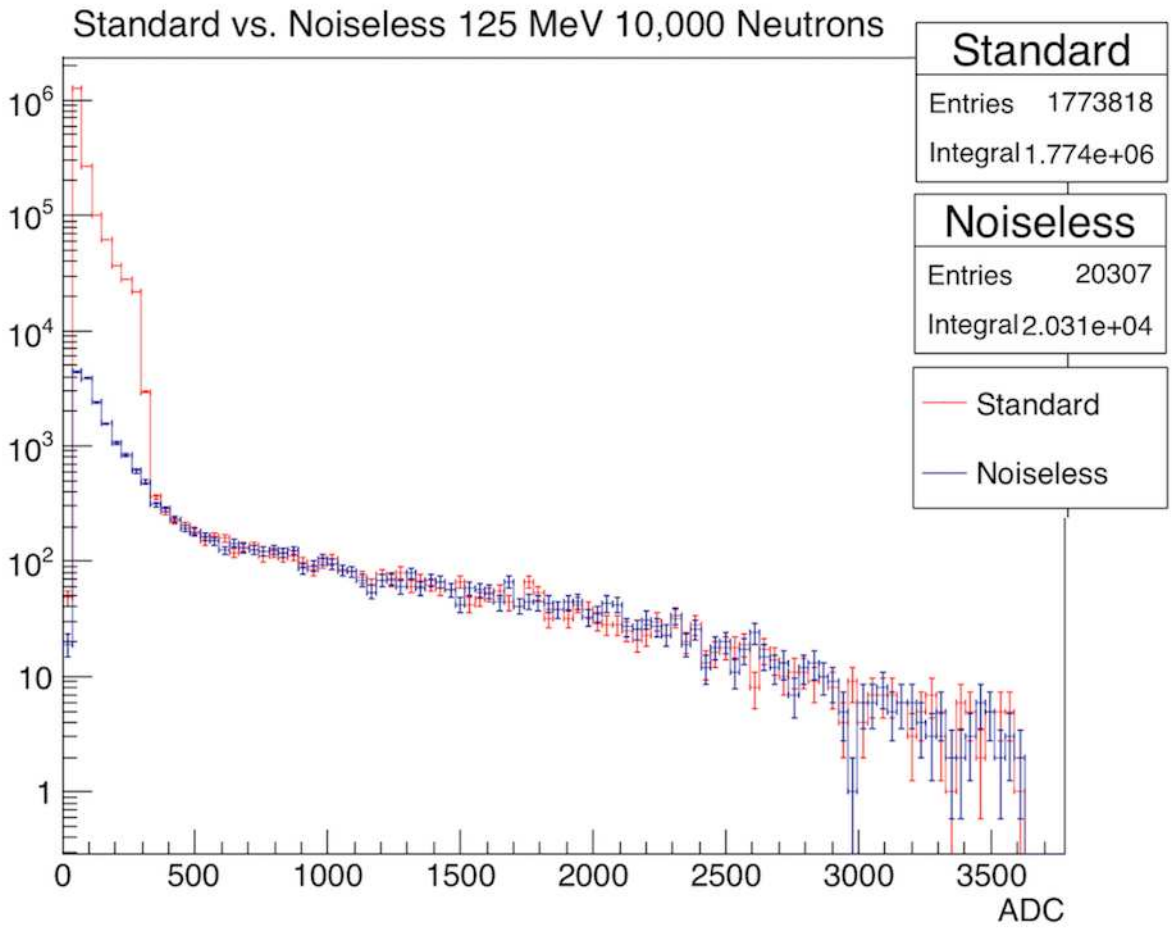

Figure A.5: Standard vs noiseless ADC per charge deposit for 10,000 neutron events at 125 MeV kinetic energy. On a semi-log plot.

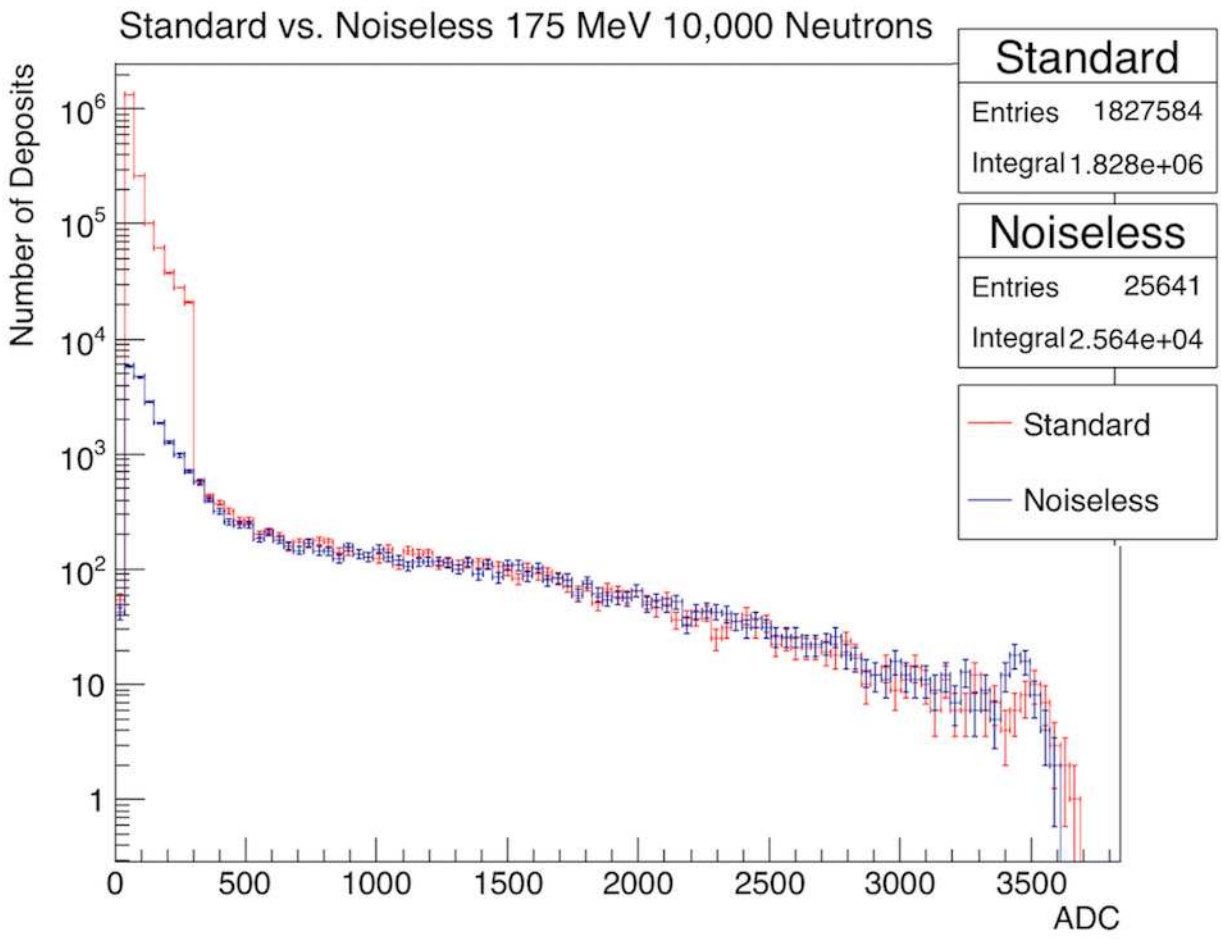

Figure A.6: Standard vs noiseless ADC per charge deposit for 10,000 neutron events at 175 MeV kinetic energy. On a semi-log plot.

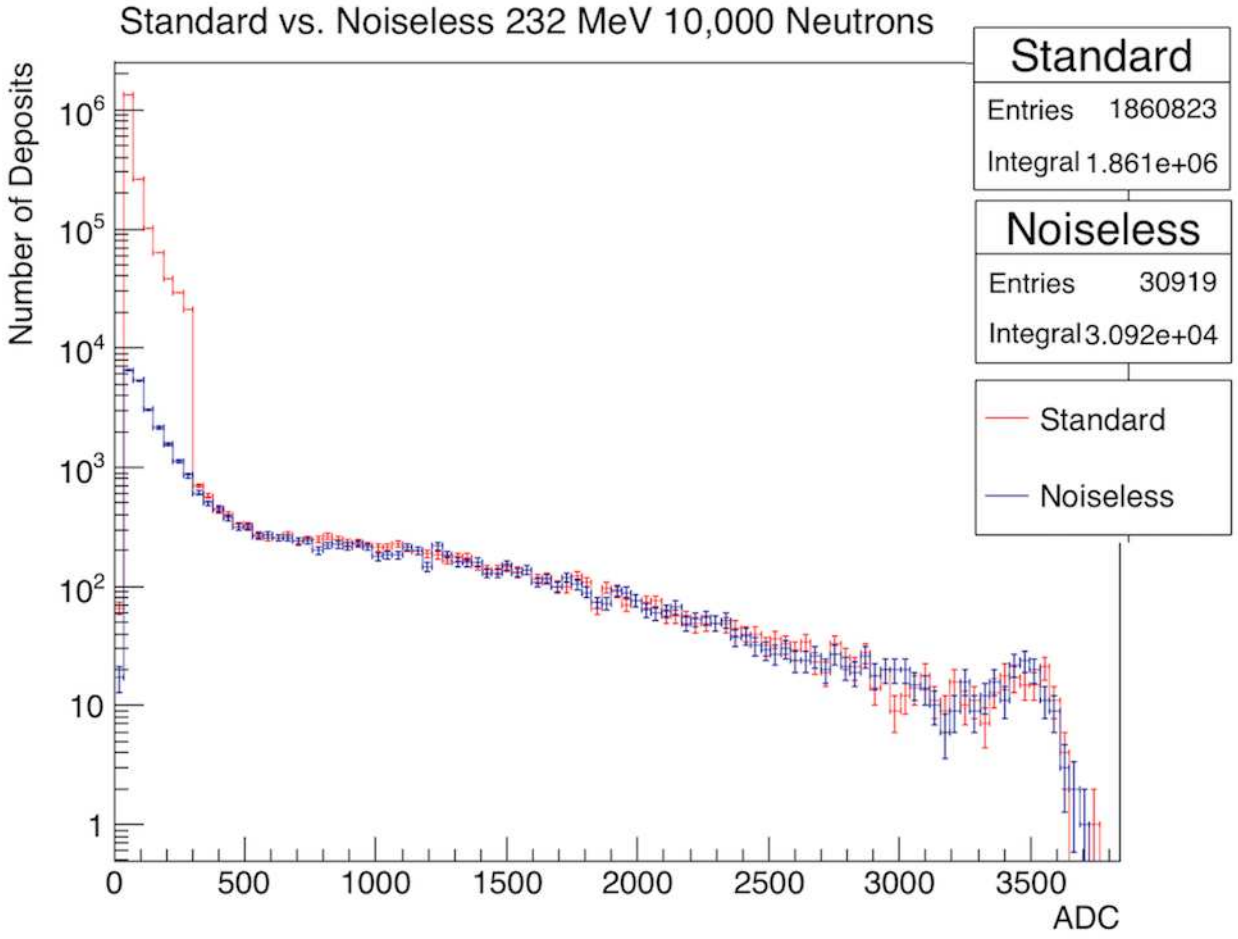

Figure A.7: Standard vs noiseless ADC per charge deposit for 10,000 neutron events at 232 MeV kinetic energy. On a semi-log plot.

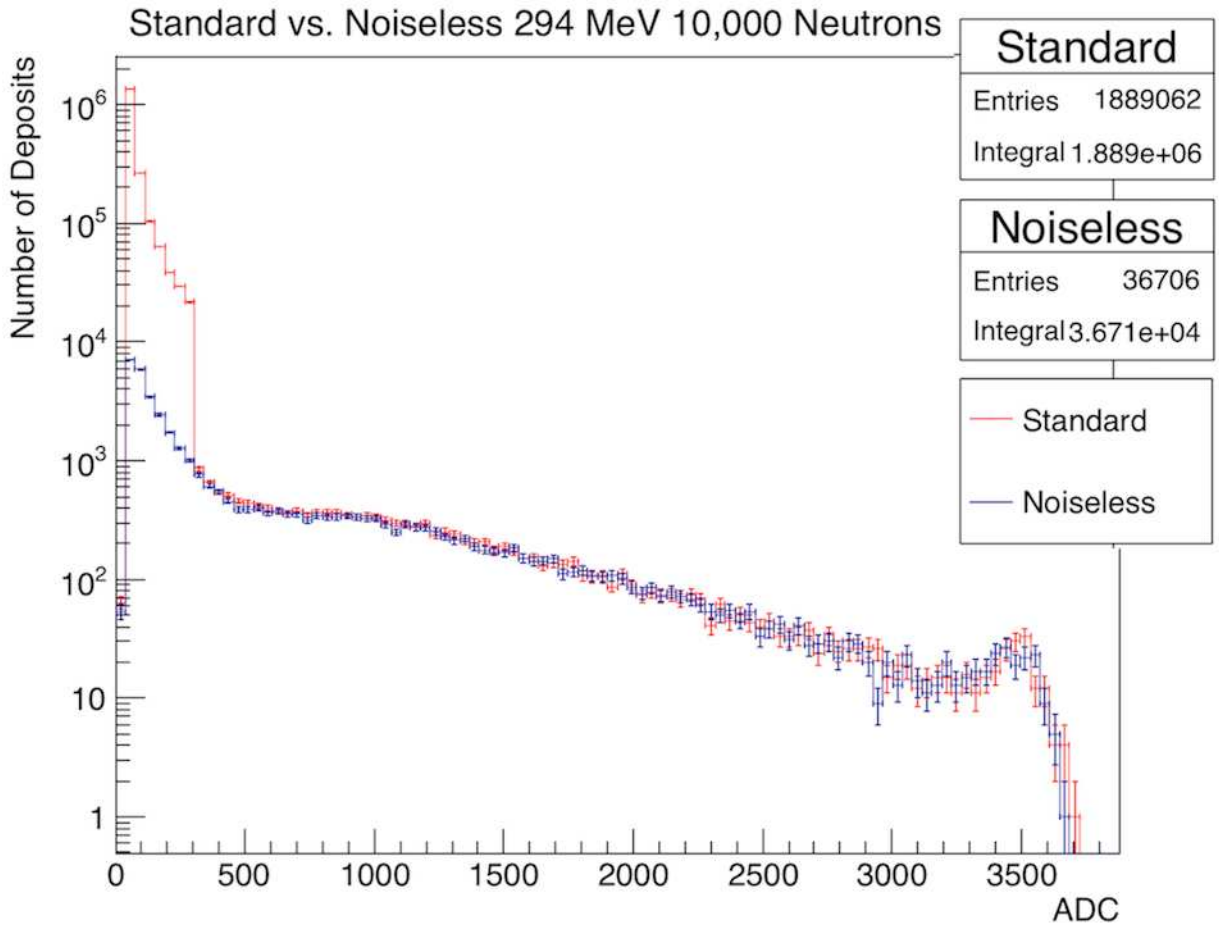

Figure A.8: Standard vs noiseless ADC per charge deposit for 10,000 neutron events at 294 MeV kinetic energy. On a semi-log plot.

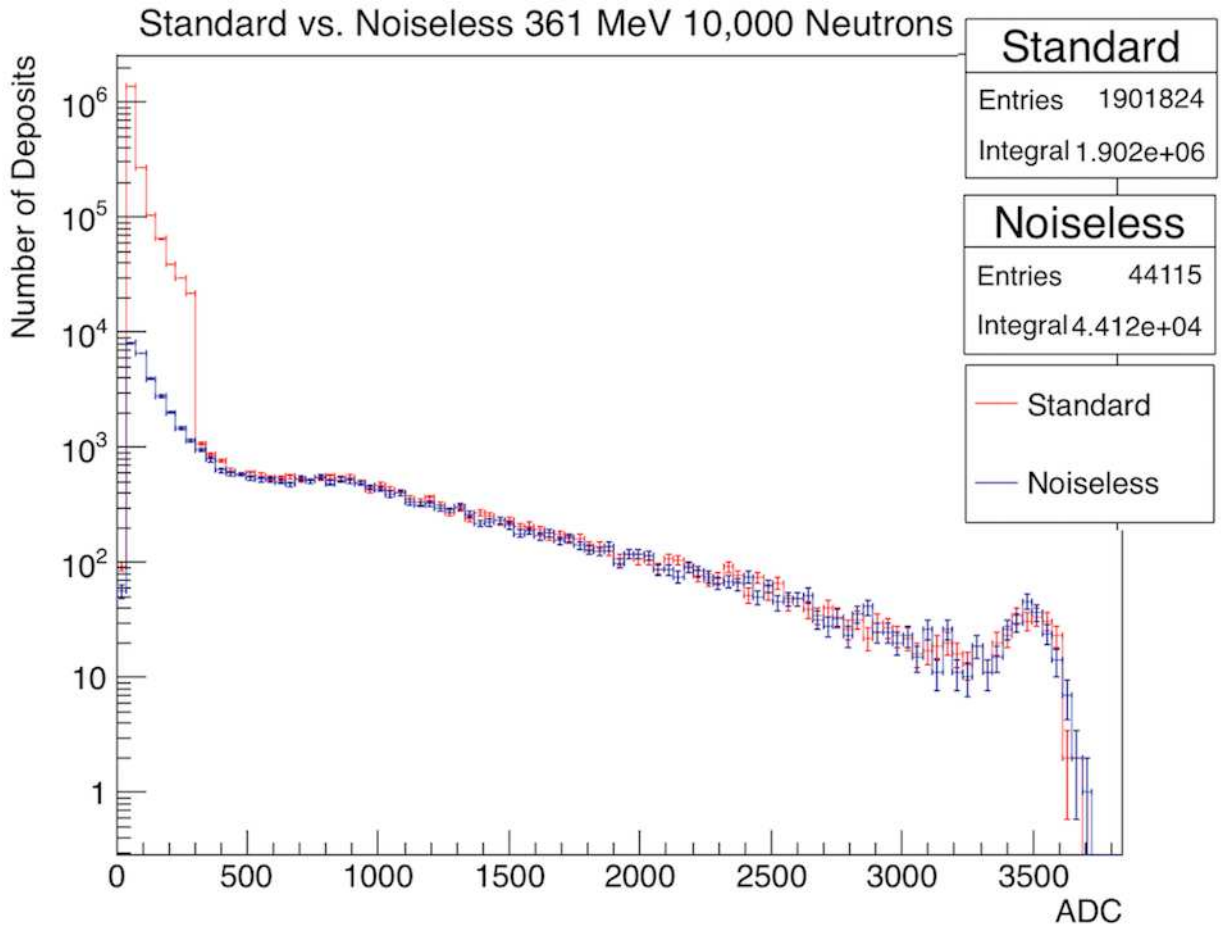

Figure A.9: Standard vs noiseless ADC per charge deposit for 10,000 neutron events at 361 MeV kinetic energy. On a semi-log plot.

List of Abbreviations

ADC	Analog-to-Digital units
APD	Avalanche Photodiode
BDT	Boosted Decision Tree
CC	Charged Current
CCQE	Charged-Current Quasi-Elastic Scattering
CNN	Convolutional Neural Network
D-T	Deuterium-Tritium
DAQ	Data Acquisition
DDT	Data Driven Trigger
ENDF	Evaluated Nuclear Data File
FD	NOνA Far Detector
GUI	Graphical User Interface
MC	Monte Carlo
NC	Neutral Current
ND	NOνA Near Detector
NOνA	NuMI Off-Axis Neutrino Appearance Experiment
NuMI	Neutrinos at the Main Injector
SM	Standard Model